Ecohydrology

WILEY

RESEARCH ARTICLE OPEN ACCESS

Seasonal Dynamics of Instream Mesohabitats Over a Long Section of a Large Subarctic River

Emmy Kärkkäinen[1] | Ville Kankare[1,2] | Jaakko Erkinaro[3] | Mikel Calle[1,4] | Harri Kaartinen[2] | Petteri Alho[1]

[1]Geography and Geology Department, University of Turku, Turku, Finland | [2]Department of Remote Sensing and Photogrammetry, Finnish Geospatial Research Institute FGI, the National Land Survey of Finland, Espoo, Finland | [3]Natural Resources Institute Finland (LUKE), Oulu, Finland | [4]Facultad de Ciencias Geológicas, Universidad Complutense de Madrid, Madrid, Spain

Correspondence: Emmy Kärkkäinen (emmy.karkkainen@utu.fi)

Received: 16 March 2026 | **Revised:** 22 July 2026 | **Accepted:** 4 August 2026

Keywords: 2D hydraulic modelling | Atlantic salmon | ecohydraulics | habitat mapping | multispectral ALS

ABSTRACT

Identifying, mapping and protecting suitable habitats are essential for species conservation. Most studies have focused on short river reaches or limited discharge scenarios. Such restricted coverage hampers effective decision-making because small-scale, short-term analyses cannot capture full habitat dynamics. This study examined mesohabitat types along a 53-km river section at 1-m xy resolution, quantified seasonal variation in mesohabitat occurrence, extent and spatial distribution across nine representative discharge scenarios derived from a 66-year daily flow record, and characterized mesohabitat class transitions between spring–summer and summer–autumn, to answer: How do typical seasonal flow dynamics during the ice-free period reorganize instream mesohabitats important for Atlantic salmon (*Salmo salar*)? Using multispectral airborne laser scanning (ALS), 2D hydraulic modelling, the Norwegian Mesohabitat Classification Method (NMCM) and spatial raster analyses, we developed an approach enabling examination of ecological phenomena that previously could not be studied on the Tana River due to limitations in high-resolution data availability with large area coverage, and/or due to discharge variability. Deep glides, pools, walks and deep rapids were the dominant mesohabitats across all discharge scenarios, but mesohabitats were also dynamic and seasonally variable. After the spring flood, the river's wetted area contracted, drying many spring mesohabitats by summer. From summer to autumn, mesohabitats were more stable, although the proportion of walk mesohabitats increased. Such seasonal dynamics have the potential to support Atlantic salmon life stages, especially spawning and juvenile rearing. The approach is broadly applicable to rivers where water clarity, turbulence and bank structure allow green-laser penetration and where reliable discharge data exist.

1 | Introduction

Because organisms tend to be more abundant where habitats support population success, identifying, mapping and protecting suitable habitats are essential for species conservation (Rosenfeld 2003; Hitchman et al. 2024). Often, effective conservation requires understanding not only where suitable instream habitats occur but also how these habitats reorganize under seasonally varying discharge regimes. In fluvial environments, physical habitats emerge from hydromorphological variables including water depth, flow velocity, bed geomorphology and substrate type. Depending on the classification method, water surface slope, surface pattern, shelter availability, embeddedness, bottom shear stress, Froude number and/or flow velocity standard deviation may also be important parameters (Borsányi et al. 2004; Eisner et al. 2005; Parasiewicz 2007; Hauer et al. 2009; Hauer et al. 2011; Vezza et al. 2014). These parameters enable classification of a river into hydromorphological units (HMUs), such as pools, riffles and runs, commonly referred to as instream mesohabitats (Parasiewicz 2007;

Alcaraz-Hernández et al. 2011). No universal minimum or maximum coverage area has been defined for a mesohabitat, but a mesohabitat is generally understood to be an area that is distinct from its surroundings and characterized by relatively homogeneous hydromorphological conditions. Positioned between microhabitats and macrohabitats, the meso-scale links fine-scale hydraulic features (e.g., flow velocity) with broader geomorphological forms (Farò et al. 2025), typically spanning one to 10 channel widths (Wyrick and Pasternack 2012).

Already, early habitat studies, such as Bisson et al. (1982), developed a classification system for salmonid habitats in small streams. While most habitat studies still focus on fish ecology (Bovee 1986; Parasiewicz 2008; O'Sullivan et al. 2020; Farò et al. 2022), applications also extend to benthic invertebrates and aquatic vegetation (Vezza, Ghia, and Fea 2016; Ochs et al. 2018; Burgazzi et al. 2021). For migratory fish that travel long distances, the meso-scale provides a more logical habitat unit than the micro-scale (Wegscheider et al. 2020). However, the dynamic behavior of mesohabitats across seasonally varying flows has remained underdocumented at long, contiguous river sections, largely due to limitations of traditional mapping approaches.

Traditionally, habitats have been mapped using field-based methods (e.g., Bisson et al. 1982; Frissell et al. 1986; Borsányi et al. 2004), capturing depth and velocity measurements across numerous river locations (Eisner et al. 2005). Although straightforward, field methods are logistically demanding, time-consuming (Eisner et al. 2005; Parasiewicz 2007), sometimes even dangerous and typically infeasible in large, nonwadable rivers (Farò et al. 2022). Challenges are encountered particularly in remote, large rivers (width > 100 m, mean discharge > 100 m^3/s). Moreover, field-based surveys capture only the habitats present at the measurement time, yet habitat occurrence varies with discharge (Borsányi et al. 2004; Hauer et al. 2009). Mapping mesohabitats across multiple discharges requires year-round surveys, making the process extremely time-consuming. In dynamic rivers, channel morphology can also change drastically after flood events (Tamminga and Eaton 2018; van Rooijen et al. 2024), necessitating frequent resurveys. Consequently, most studies have focused on short river reaches (Fausch et al. 2002; Wyrick et al. 2014) or limited discharge scenarios. For migratory fish with large spatial requirements, such restricted coverage is problematic, as small-scale studies over short time frames fail to support conservation decision-making (Fausch et al. 2002). To better understand mesohabitat distribution, mapping should encompass long river reaches under multiple flow conditions, but the necessary field data remain time-intensive to collect.

To overcome these limitations, two-dimensional (2D) hydraulic modelling has become increasingly common in habitat studies (Hauer et al. 2009; Wyrick et al. 2014; Mandlburger et al. 2015; Farò et al. 2022; Yu et al. 2025). These models capture detailed spatial flow patterns across discharges (Nelson et al. 2003; Lamouroux et al. 2017). Depth-averaged 2D models offer a balance of computational efficiency and spatial accuracy (Hauer et al. 2013), improving habitat quantification over one-dimensional (1D) models while being more computationally feasible than three-dimensional (3D) models (Sinha et al. 1998). Building a 2D hydraulic model still requires topographic data and comprehensive calibration data, including digital terrain models (DTMs) and water-level or velocity measurements. Acquisition of such data remains a major challenge, and the availability of high-resolution DTMs often limits hydraulic modelling applications (Hauer et al. 2009; Jowett and Duncan 2012; Wyrick et al. 2014). However, recent advances in remote sensing offer a promising solution.

Remote sensing techniques are increasingly used to generate comprehensive DTMs (Kuiper et al. 2023) covering entire river sections. Unmanned aerial vehicles (UAVs), such as drones, have become popular tools for habitat mapping (Vezza et al. 2016; Woodget et al. 2017). However, optical techniques require reference topo- and bathymetric measurements alongside aerial imagery (Hugue et al. 2016). In contrast, airborne laser scanning (ALS) directly produces accurate 3D point clouds for capturing terrain and surface characteristics (Bakuła 2015). ALS is unaffected by shading or relief distortions, unlike optical techniques (Kasvi et al. 2019). ALS can rapidly cover extensive areas without contacting the water, enabling data collection even in fast-flowing or shallow reaches. Nevertheless, conventional topographic ALS uses near-infrared (NIR) wavelengths (typically 1064 or 1550 nm), which cannot penetrate water due to refraction and absorption (Farò et al. 2025). Thus, NIR-based ALS provides only topographic data, excluding river bathymetry. Supplementing ALS with boat-based depth surveys is possible (e.g., Wyrick and Pasternack 2012), but this negates the advantages of ALS and complicates the creation of continuous DTMs for long river sections. Bathymetric capability is therefore essential.

Bathymetric mapping is feasible with green-wavelength lasers (typically 532 nm), which penetrate water and can capture bathymetry at high resolution and broad spatial scales (McKean et al. 2009; Tonina et al. 2019). Multispectral ALS combines NIR and green lasers, enabling simultaneous mapping of floodplain topography, water surface and submerged terrain. Initially developed for terrestrial applications (Takhtkeshha et al. 2024), multispectral ALS has proven valuable in aquatic environments. It enhances depth mapping (Fernandez-Diaz et al. 2016), facilitates water-land separation (Morsy et al. 2018), and supports water-surface detection (Yan et al. 2018). Furthermore, improved canopy discrimination assists vegetation filtering (Glennie et al. 2013), further enhancing DTM quality. These advances allow established habitat classification methods to be applied at unprecedented spatial and temporal scales. However, multispectral ALS remains a relatively new technology in river studies.

Despite technological progress, most habitat studies still focus on short reaches (less than a few kilometres), moderately small and wadable rivers (mean discharge < 100 m^3/s) and limited flow scenarios. Many focus on either low-flow or flood conditions (Tamminga and Eaton 2018; van Rooijen et al. 2024) or consider only a single discharge (O'Sullivan et al. 2020), often in regulated rivers (Wyrick and Pasternack 2012; Mandlburger et al. 2015). Even when multiple discharges (Hauer et al. 2009) or long reaches (Yu et al. 2025) are analysed, natural seasonal patterns are seldom addressed.

In northern regions, strong hydrological seasonality can substantially alter habitat use by fluvial and anadromous fish

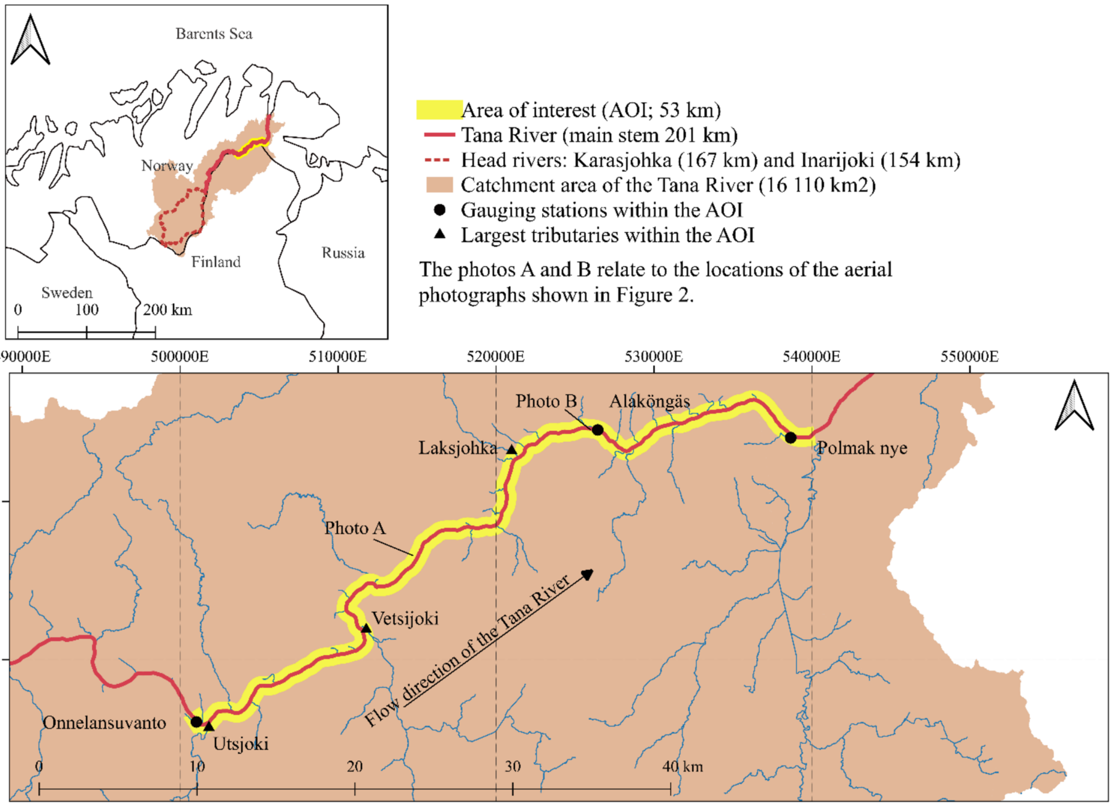

FIGURE 1 | The location of the Tana River catchment and area of interest (AOI). The map coordinates are in ETRS-TM35FIN.

species. The large subarctic Tana River in the northernmost part of Europe supports several fish species, but the river is especially renowned for its large, diverse Atlantic salmon (*Salmo salar*) population complex (Erkinaro et al. 2019). Seasonal habitat use of Atlantic salmon varies across life stages—from autumn spawning (Louhi et al. 2008) to egg development and alevin hatching in summer to habitat segregation among juvenile age classes (Linnansaari et al. 2010; Metsäniemi et al. 2025). The previous Tana River mesohabitat study (Metsäniemi et al. 2025) used the field-based Norwegian Mesohabitat Classification Method (NMCM) (Borsányi et al. 2004), in which the classification relies on hydraulic thresholds. Although widely applied in Norway for salmon rivers, NMCM—like other field-based approaches—faces challenges related to subjective threshold identification, limited temporal resolution and inconsistent habitat boundaries (Wyrick et al. 2014). Modelling can reduce such subjectivity (Wegscheider et al. 2020). Moreover, multispectral ALS and 2D hydraulic modelling offer a solution to the issues listed above while remaining compatible with NMCM, allowing comparison with earlier NMCM-based results.

Metsäniemi et al. (2025) emphasized the need for dynamic, spatiotemporally explicit habitat assessments. In summary, we still lack mesohabitat studies that simultaneously cover long, continuous river sections, rely on high-resolution, spatially continuous topographic and bathymetric data, encompass multiple, naturally occurring discharge levels rather than only one or a few flows and capture typical patterns of seasonal habitat reorganization. This knowledge gap is particularly pronounced in large, nonwadable and near-pristine subarctic rivers. Integrating NMCM with spatially continuous, multidischarge hydraulic modelling enables evaluation of mesohabitat expansion, contraction and transitions under seasonally varying flows across entire river reaches. This shifts classification from a static depiction to a dynamic analytical framework, supporting ecological inference. Motivated by this perspective, this study aims to examine seasonal dynamics of mesohabitats along the near-pristine, subarctic Tana River using multispectral ALS, 2D hydraulic modelling and NMCM. Specifically, we (1) identify mesohabitat types along a 53-km river section at 1-m xy resolution, (2) quantify seasonal variation in mesohabitat occurrence, extent and spatial distribution across nine representative discharge scenarios derived from a 66-year daily discharge record and (3) characterize mesohabitat class transitions between spring–summer and summer–autumn. To clarify the value of mesohabitat mapping, our final research question becomes: How do typical seasonal flow dynamics during the ice-free period reorganize the occurrence and extent of instream mesohabitats important for wild Atlantic salmon when mapped continuously across space and across multiple discharges?

2 | Data and Methods

2.1 | Study Area

The study was conducted on the subarctic Tana River (*Teno* in Finnish and *Deatnu* in Sámi), which forms the border between Finland and Norway (68–70°N, 25–27°E) (Figure 1, Figure 2). The Tana River main stem spans 201 km, originating from the confluence of Karasjohka (~167 km) and Inarijoki (~154 km) and flowing into the Barents Sea. The catchment area is 16,110 km^2, of which 31.8% lies in Finland and 68.2% in Norway. Land cover includes forests and treeless highlands (72%), wetlands and lakes (16%), agricultural land (0.2%), urban areas (0.1%) and other land uses (12%). The river is unregulated, with minimal human impact, high water quality and low turbidity.

The Tana River catchment belongs to the Köppen-Geiger climate class Dfc: 'Snow climate, fully humid (no dry season), with cool summer and cold winter' (Kottek et al. 2006). The annual hydrological cycle of the Tana River basin follows the typical pattern of subarctic regions, where snow accumulation, spring flood peaks and summer and autumn rainfall dictate the flow rates (Figure 3). The Tana River typically freezes in November, and the freezing period lasts approximately 6 months until May. During this period, precipitation typically occurs in the form of snow. Peak discharge occurs shortly after ice breakup, generally from mid-May to early June, and is caused by spring snowmelt. More detailed hydrological data on the Tana River's discharge are presented in Section 2.2.2.

Geomorphologically and hydraulically, the river can be divided into the following three sections: upper, middle and lower course

FIGURE 2 | The Tana River in September 2022. The locations where the photos were taken are marked in Figure 1.

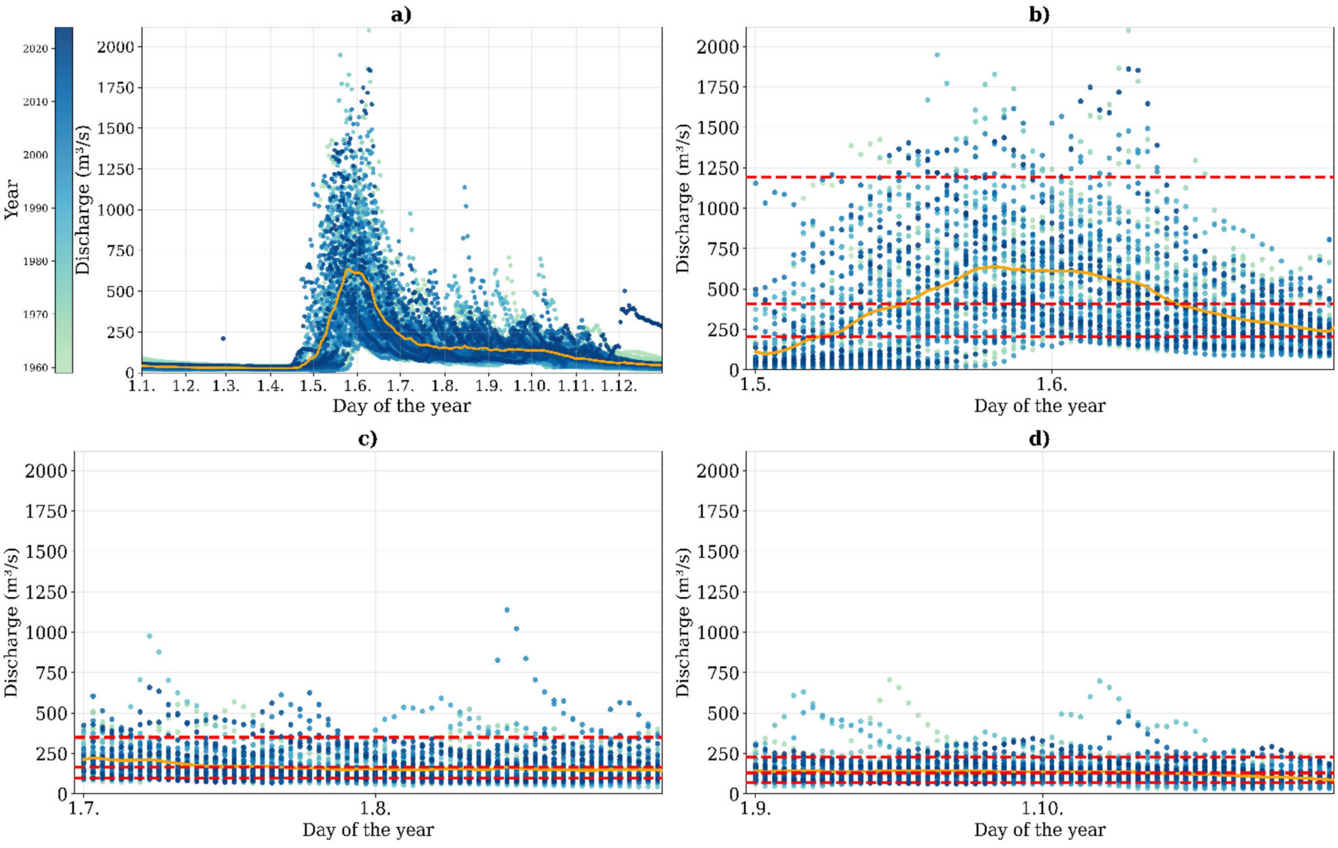

FIGURE 3 | Tana River discharge at the Onnelansuvanto gauge station from 1959 to 2024: (a) all daily discharge measurements for 66 years, (b) daily discharge measurements for the springs (May–June), (c) daily discharge measurements for the summers (July–August) and (d) daily discharge measurements for the autumns (September–October). Older results are shown in lighter green and newer results in darker blue. Yellow lines are daily averages, and red lines are mean (MQ), mean-high (MHQ) and mean-low (MNQ) discharges for the seasons. In the image, dates are in day-month format.

(Mansikkaniemi 1970). The upper and lower sections feature sandbars with shallow, slow-flowing waters, while the middle section is characterized by a gravel bed, rocky riverbanks and rapids of varying intensity. The middle section exhibits natural armoring, where coarse material protects the riverbed and reduces erosion, whereas the lower reaches include erodible sand, silt and clay (Collinson 1970).

The area of interest (AOI) was a 53-km reach from *Utsjoki* to *Polmak* (Figure 1), encompassing both the middle and lower sections. The AOI included major tributaries such as *Utsjoki*, *Vetsijoki* and *Laksjohka*, and featured the *Alaköngäs* rapid. During average autumn discharge, the river width ranged from ~60 to ~650 m, with an average depth of ~1.3 m. At the downstream boundary of the AOI, the catchment area was 14,340 km^2. The AOI was delineated due to the availability of high-resolution multispectral ALS data and long-term hydrologic records from the *Onnelansuvanto* and *Polmak nye* gauge stations.

The Tana River is among the world's most biologically diverse salmon rivers (Erkinaro et al. 2019) and is culturally significant for the indigenous Sámi people (Hiedanpää et al. 2020). According to the Tana/Teno Monitoring and Research Group (MRG) 2026 report, the river is unaffected by the highest-priority threats to salmon stocks in Norway: There is no hydropower regulation, water diversion, acidification, pollution or mining and physical alterations are minimal; agricultural and community runoff is limited, and no harmful parasites are present (Anon 2026). Despite the near-pristine catchment, Atlantic salmon populations have declined over the past decade, likely due to drastically decreased marine survival rates (Anon 2026), affecting local communities dependent on salmon fishing (Hiedanpää et al. 2020).

2.2 | Data

2.2.1 | Multispectral Airborne Laser Scanning Data

The primary dataset comprised multispectral airborne laser scanning (ALS) data collected on 7th, 8th and 10th September 2022 by the Finnish Geospatial Research Institute (FGI) using the helicopter-based HeliALS-TW system. The system included three laser scanners—Riegl VUX-1HA, miniVUX-3UAV and VQ-840-G (Riegl GmbH, Austria)—operating at wavelengths of 1550, 905 and 532 nm, respectively. The ranging accuracy of the scanners was 5, 15 and 20 mm, respectively. These were complemented by a GNSS-IMU navigation system consisting of a NovAtel (LITEF) ISA-100C inertial measurement unit, a NovAtel PwrPak7 GNSS receiver and a NovAtel (Vexxis) GNSS-850 antenna. This configuration has not previously been used in fluvial research. The survey covered the river channel and adjacent floodplains (~50–150 m wide) during low autumn water levels to maximize point cloud quality. In this case, quality maximization meant maximizing the number of reflections collected from dry land, as the number of ground hits decreases when the laser hits water, as only the green wavelength of VQ-840-G has the potential to penetrate below the water surface. Flight altitude was 100–150 m above ground at 20–25 m/s. Data acquisition exploited the preview of VQ-840-G's elliptical scan geometry for flight line optimization: The helicopter first followed one shore and then flew additional lines along the river to achieve full channel coverage. The VUX and mini-VUX scanners were tilted 15° to maximize hits on the vertical structures in flight direction.

Despite the multispectral approach, ALS has limitations: Green-laser penetration requires low turbidity, low suspended sediment, minimal turbulence and vegetation and no ice cover (Kasvi et al. 2019; Legleiter and Harrison 2019; Tonina et al. 2019). A green laser can penetrate to approximately one to three Secchi depths (Mandlburger 2025). Two deeper areas (0.33 km^2 in total, covering ~2% of the wetted area of Spring mean high discharge scenario) produced errors in our survey, but they were identifiable and corrected manually during DTM creation. In addition, ALS cannot resolve undercut banks, and ALS data also age when sediment transport alters the riverbed.

Trajectory processing used Waypoint Inertial Explorer (NovAtel Inc. 2020). Basic point-cloud processing was done with RiProcess, followed by flight-line tuning with RiPrecision and bathymetric processing with RiHydro. The resulting point clouds were further processed in Terrascan: Low and isolated points were filtered out, and ground points were classified with Terrascan's ground classification tool using only points with echo parameter 'last-of-many' and 'only.' Within the AOI (channel, banks and floodplains), the average density of points classified as ground was 3.96 points/m^2 (average spacing of 0.5 m). Taking the prementioned scanner ranging accuracies and the trajectory postprocessing result into account, individual laser scanning point elevation accuracy was estimated to be about 5 cm for bare ground and about 10–15 cm for underwater surfaces. A 1-m xy resolution DTM was generated from ground returns using *blast2dem* tool in the LAStools software (Rapidlasso GmbH), which triangulates the point cloud, and rasters it into a DTM. The DTM was used as the terrain geometry for hydraulic modelling, while water surface returns supported hydraulic model calibration.

2.2.2 | Hydrological Data

Hydrological data were obtained from the Finnish Environment Institute (Syke) and the Norwegian Water Resources and Energy Directorate (NVE). Syke has monitored discharge and water level at *Onnelansuvanto* since 1959; NVE has operated *Polmak nye* since 1991 (Figure 1). Syke has also measured discharge at *Patoniva* (69° 47,022′ N, 26° 59,973′ E) on the Utsjoki River since 1962. Stations provide daily measurements with open access (see Data Availability Statement).

From 1 January 1959 to 31 December 2024, the average discharge at *Onnelansuvanto* was 139 m^3/s (Figure 3), with an average water level of 64.27 m (N2000).

2.2.3 | Aerial Photographs

In September 2022, low-altitude (1 and 2 m) aerial photographs (Figure 4) were captured by a DJI Mavic Mini2 drone at 10 locations within the AOI. The camera was 12MP, model FC7303. The drone had a GPS device, but not a real-time kinematic

FIGURE 4 | Examples of aerial photographs from the Tana River in September 2022. The length of one side of the scale bar in the photographs is 60 cm. In the left photograph, the substrate mainly consists of cobbles (< 300 mm) and boulders (> 300 mm), while in the right photograph it consists of sand (< 2 mm).

(RTK) GPS system. Images revealed substrate types including sand (< 2 mm), gravel (< 16 mm), pebbles (< 64 mm), cobbles (< 300 mm) and boulders (> 300 mm). Visual interpretation of the aerial photographs informed the initial estimation of riverbed roughness (Manning's *n*) values applied in the hydraulic model.

2.3 | Hydraulic 2D Modelling

2.3.1 | Model Setup

A 2D hydraulic model for the AOI was developed using HEC-RAS 6.6 software (US Army Corps of Engineers Hydrologic Engineering Center). The model employs an implicit finite volume method based on Shallow Water Equations. Such 2D models simulate spatial patterns of depth-averaged flow and are widely used in mesohabitat studies (e.g., Hauer et al. 2009; Gibson and Pasternack 2015). Model terrain geometry was derived from the 1-m DTM built from multispectral ALS data. The AOI was divided into ~735,700 cells, with mesh element sizes of ~25 m^2 in the channel and active floodplains, and ~10,000 m^2 in inactive floodplains. This configuration balanced computational accuracy with runtime constraints, given the limitations of the available hardware. HEC-RAS employs a subgrid bathymetry approach that preserves high-resolution DTM information within each computational cell (Casulli 2008; Elbashir 2019), enabling mesohabitat mapping at the native resolution (1 m). Consequently, the results of the 2D hydraulic model represented spatially averaged values over 1-m^2 areas.

Upstream boundary conditions used discharge from the *Onnelansuvanto* and *Patoniva* gauge stations. The Normal Depth method with a slope of 0.001 defined the downstream boundary condition. In most scenarios, the combined discharge of *Onnelansuvanto* and *Utsjoki* exceeded discharge at *Polmak nye*, indicating minimal influence from other tributaries.

2.3.2 | Calibration

During the calibration phase, the riverbed roughness—Manning's *n* values—was adjusted to match simulated water levels to measured water surface elevations (WSEs) derived from multispectral ALS data, collected on 8th September 2022. At that time, discharge was 133 m^3/s at *Onnelansuvanto* and 23 m^3/s at the Utsjoki mouth. Twenty-seven WSEs along the thalweg, spaced 2 km apart, were selected (Figure 5). Elevations were averaged from ALS points within 60-m-wide and 0.1-m-long transects. The transects were deliberately short in the direction of flow due to rapid longitudinal water-level change, and wide to maximize the number of laser points considered. All ALS calibration points were manually verified in CloudCompare by comparing their elevations with ground-point elevations. Observed water level at *Polmak nye* was also used, yielding 28 WSEs in total, 27 of which were based on 4461 individual laser points.

Initially, using only a single Manning's *n* value for the entire channel area was tested, but it did not produce good calibration results. Spatially distributed *n* values improve model performance (Baumgartner 2020), although they increase computation time. To avoid overcomplicating the calibration, we used the smallest possible number of *n* values: 0.035–0.13 for the channel (Figure 5) and 0.1 for vegetation (riparian trees and shrubland). The same Manning *n* value was used across the entire width of the channel cross-section, but depending on the calibration results, consecutive segments could have the same or different *n* values. At the *Alaköngäs* rapid, it was necessary to use *n* values that were exceptionally high for a natural river (0.11 and 0.13) to ensure that the simulated water level corresponded to the measured water level at an acceptable level. The *Alaköngäs* rapid has a steep gradient (slope of 0.00357; Mansikkaniemi 1970) and highly turbulent water; therefore, there is uncertainty regarding both the measured and simulated water levels in the rapid area. Simulated water levels differed from measured WSEs by 1.0–22 cm, with a mean squared error (MSE) of 0.007 cm^2, root mean square error (RMSE) of 8.4 cm, mean absolute error (MAE) of 6.9 cm, correlation $r = 0.999$ and coefficient of determination $R^2 = 0.999$.

2.3.3 | Discharge Scenarios

The calibrated 2D hydraulic model was used to simulate nine steady-state discharge scenarios (Table 1) representing the ice-free period and key phases of the Atlantic salmon life cycle—spring (May–June), summer (July–August) and autumn

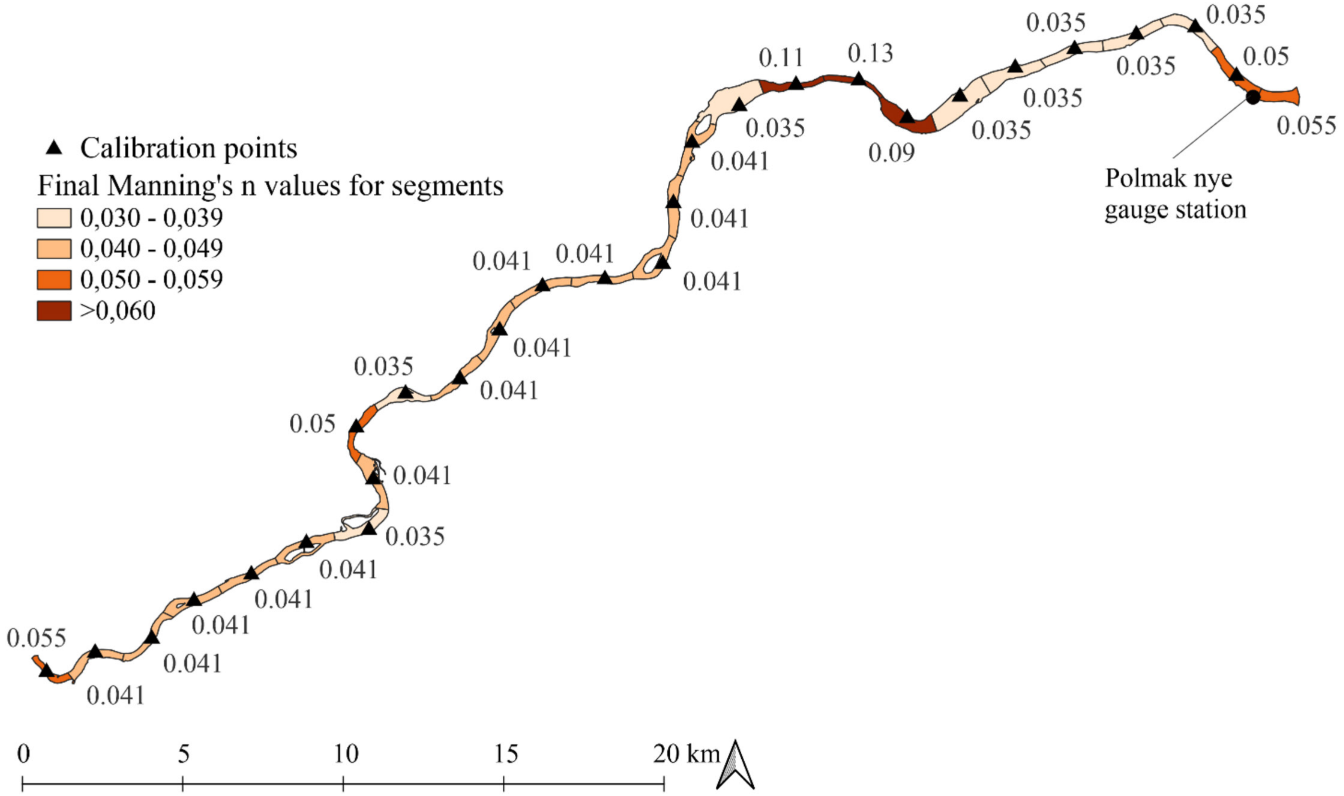

FIGURE 5 | Final Manning's *n* values used in the channel area in different segments, and calibration points within the AOI.

TABLE 1 | Calibration parameters, scenario values and catchment areas used for boundary conditions. Discharge values shown in parentheses are derived from the Onnelansuvanto gauge station time series.

Description	**Reference day**	**Discharge in the *Onnelansuvanto* (m^3/s)**	**Discharge in the mouth of Utsjoki (m^3/s)**
Model calibration	8-Sep-22	133	23
Spring MHQ (1191 m^3/s)	25-May-22	1188	220
Spring MQ (407 m^3/s)	9-Jun-22	417	47
Spring MNQ (207 m^3/s)	21-Jun-22	213	27
Summer MHQ (349 m^3/s)	22-Jul-22	353	37
Summer MQ (167 m^3/s)	4-Jul-22	168	21
Summer MNQ (97 m^3/s)	7-Jul-23	97	13
Autumn MHQ (230 m^3/s)	18-Sep-22	230	38
Autumn MQ (130 m^3/s)	9-Sep-22	129	23
Autumn MNQ (69 m^3/s)	14-Sep-24	69	8
Description		***Onnelansuvanto* (km^2)**	**Utsjoki mouth (km^2)**
Catchment area		10701.641	1657.626

(September–October). The selected scenarios are based on 24,090 individual measurements and derived statistical summaries. For each season, mean (MQ), mean-high (MHQ) and mean-low (MNQ) discharge conditions were derived from the 66-year time series of *Onnelansuvanto* (Figure 3; Table 1). MHQ was the mean of the highest daily discharge values in the single years during defined season, and MNQ the mean of the corresponding minima. As an exception to the above, the spring MNQ of 56 m^3/s reached the limit of model capacity. Very low early-May flows likely occurred while the river was still partially frozen; therefore, spring MNQ was recalculated excluding discharge values before the spring-flood peak, yielding 207 m^3/s. Winter conditions (November–April) were excluded.

TABLE 2 | The Norwegian Mesohabitat Classification Method (NMCM) used in the study (Borsányi et al. 2004) as an exception; in our study, we used a Froude number (Fr) of 0.25 as the threshold value for the surface pattern and 1.5% as the threshold value for the surface gradient. The threshold values refer to the average for the area being classified. Mesohabitat names are from Metsäniemi et al. (2025).

Criteria	Surface pattern	Surface gradient	Surface velocity	Water depth	Mesohabitat class	Mesohabitat name
Decision	Smooth/rippled (Fr < 0.25)	Steep > 1.5%	Fast > 0.5 m/s	Deep > 0.7 m	A	Run
		Moderate < 1.5%	Fast > 0.5 m/s	Deep > 0.7 m	B1	Deep glide
				Shallow < 0.7 m	B2	Shallow glide
			Slow < 0.5 m/s	Deep > 0.7 m	C	Pool
				Shallow < 0.7 m	D	Walk
	Broken/unbroken standing waves (Fr > 0.25)	Steep > 1.5%	Fast > 0.5 m/s	Deep > 0.7 m	E	White water
				Shallow < 0.7 m	F	Cascade
		Moderate < 1.5%	Fast > 0.5 m/s	Deep > 0.7 m	G1	Deep rapid
				Shallow < 0.7 m	G2	Shallow rapid
			Slow < 0.5 m/s	Shallow < 0.7 m	H	Rill

Scenarios were constructed using reference days: After computing seasonal mean discharges, we identified dates in the discharge record with comparable values. This ensured that each scenario represented typical seasonal conditions while remaining grounded in realistic, observed flow states. The approach also preserved the empirical linkage between Tana River and Utsjoki River discharges, improving model consistency and reliability. To account for spring-flood effects on channel morphology, reference dates were primarily drawn from the period between the 2022 and 2023 spring floods. Exceptions (Spring MHQ, Summer MNQ and Autumn MNQ) were made when seasonal flows in that interval did not reflect long-term averages, in which case dates from other recent years with comparable discharges were selected.

Model outputs—WSE, flow velocity, water depth and Froude number—were exported as 1-m rasters covering the AOI and imported into QGIS 3.34.8 for spatial raster analyses.

2.4 | Mesohabitat Classification and Spatial Raster Analyses

In order to map the mesohabitats, the results of the hydraulic model had to be classified. The following four main methods exist for instream mesohabitat classification: the Mesohabitat Evaluation Model (MEM) (Hauer et al. 2009; Hauer et al. 2011), NMCM (Borsányi et al. 2004), MesoCASiMiR (Eisner et al. 2005; Wegscheider et al. 2024) and MesoHABSIM (Parasiewicz 2007; Vezza et al. 2014). In this study, the mesohabitat patches were delineated from 1-m^2 hydromorphological cells using the NMCM. We applied NMCM to ensure comparability with a previous field-based study in the Tana River (Metsäniemi et al. 2025) and to avoid introducing new typologies that hinder cross-study comparison (Wheaton et al. 2015). NMCM uses a threshold-based decision tree to classify habitats into ten categories (Table 2).

Field-based mesohabitat studies are often based on determining averages for large areas. Our approach differed from this, as we defined mesohabitats such that all 1-m^2 cells met the same criteria (Table 2). Thus, the mesohabitats we mapped are hydraulically homogeneous.

The NMCM is designed for in situ classification based on visual observation, with its initial steps optimized for human interpretation. However, surface-pattern identification is challenging to reproduce from broad-scale 2D hydraulic models. To address this, we used the Froude number (Fr) raster exported from HEC-RAS, where Fr for each cell is computed from depth and flow velocity:

$$Fr = \frac{v}{\sqrt{gd}} \quad (1)$$

where v is flow velocity (m/s), g is the gravitational constant (9.81 m/s^2), and d is water depth (m). The Froude number is a dimensionless indicator that has been empirically shown to distinguish pools (smooth surface) from rapids (broken surface) (Jowett 1993), which aligns with NMCM's surface-pattern criterion. Hauer et al. (2009) have also noted that the Froude number indicates a strong correlation between the development of low-energy habitats and high-energy habitats, and is potentially a useful variable for characterizing aquatic habitats. We classified the Froude raster into Fr $\leq$0.25 (smooth) and Fr $>$0.25 (broken) (Figure 6), informed by Finnish topographic maps (National Land Survey of Finland 2024) and aerial imagery (National Land Survey of Finland 2015), and supported by literature (e.g., Jowett 1993; Newson et al. 1998; Hauer et al. 2009; Entwistle et al. 2019). Water-surface gradient was derived from the surface-elevation raster and classified into moderate and steep ($\leq$1.5% and $>$1.5%) (Figure 6). Regarding the threshold value for the surface gradient criterion, we deviated slightly from the value proposed by NMCM. Borsányi et al. (2004) noted that threshold values should be viewed critically

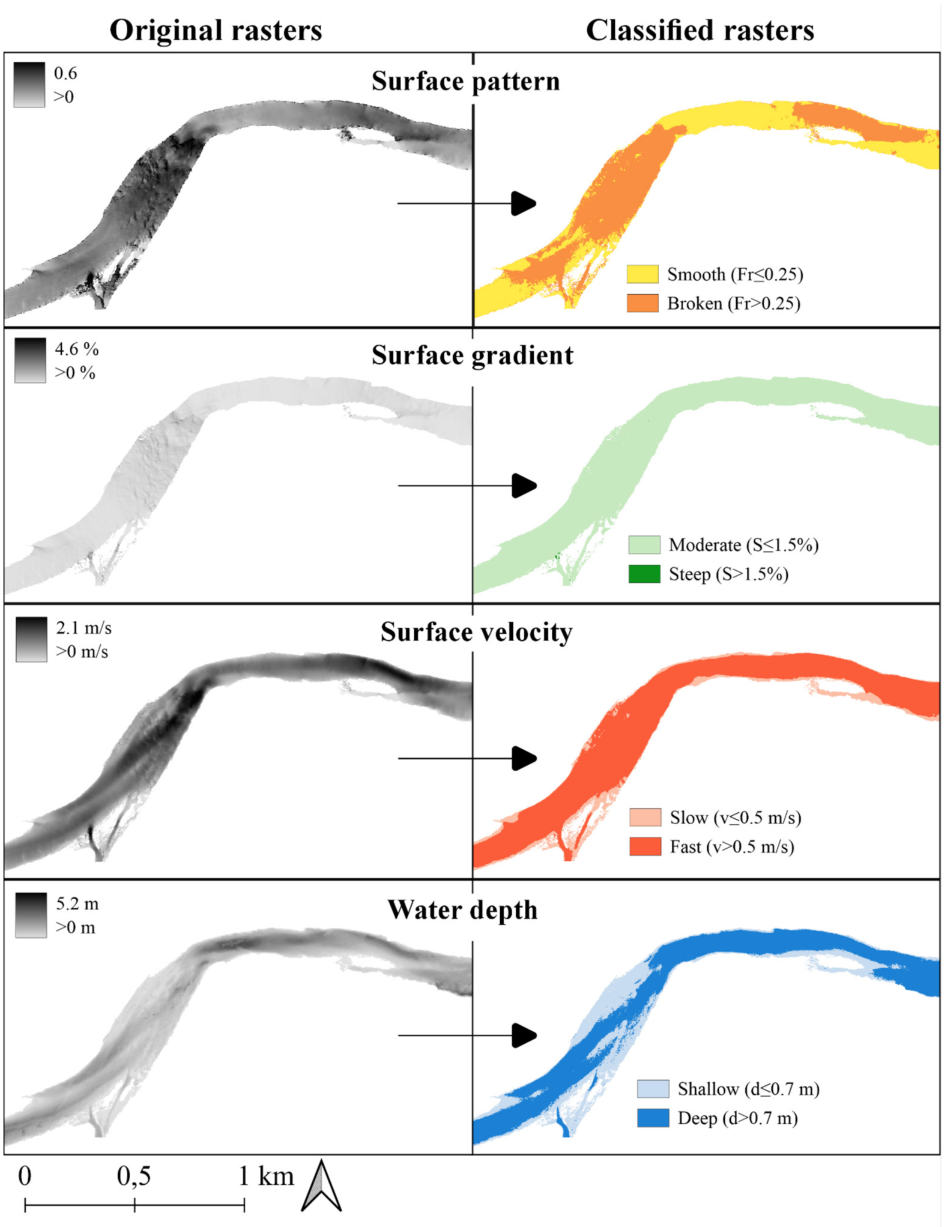

FIGURE 6 | Example of four original and classified rasters from the Autumn MQ scenario. The classified rasters were subsequently combined for mesohabitat classification. The figure illustrates a short reach spanning a few kilometres of the AOI. The minimum and maximum values of the parameters in the entire AOI are shown in the original rasters (left). All maps share the same scale and orientation.

and that larger rivers, in particular, may require adjustments to these values. Surface gradient strongly influences the occurrence of run, white water and cascade mesohabitats, with white water and cascade habitats moderately identifiable from aerial imagery. We therefore tested several surface gradient thresholds between 1% and 4% and compared the resulting habitat classifications with aerial imagery (National Land Survey of Finland 2015; Geovekst 2019; Google Earth, n.d.). Although no imagery contemporaneous with the point cloud data was available, white water areas in the Tana River were observed to occur largely in the same locations across seasons and years; consequently, the aerial images worked well for adjusting the surface gradient criterion. Water depth and flow velocity rasters were similarly classified into shallow/deep (≤/> 0.7 m) and slow/fast (≤/> 0.5 m/s) classes, respectively (Figure 6). The threshold values for water depth and flow velocity were chosen to be the same as those used by Metsäniemi et al. (2025), as we wanted to ensure the comparability of our studies. It should be noted that NMCM uses the surface velocity, whereas the HEC-RAS model produces the depth-averaged mean velocity. The typical flow velocity profile in an open channel indicates that the flow velocity at the surface is always higher than the mean velocity. Conversion of the depth-averaged mean velocity to surface velocity was obtained using a constant velocity coefficient (α) 0.85. Although the α value is site-specific, Welber et al. (2016) demonstrated that the default value 0.85 works well in a variety of rivers. Ultimately, pixels in each raster were assigned new values based on classification.

The four classified rasters (Figure 6) were combined by multiplying the per-pixel codes:

$$M = a_{Fr} \times b_S \times c_v \times d_d \quad (2)$$

where a_{Fr}, b_{S}, c_{v} and d_{d} denote the dimensionless, per-pixel codes for Froude number, surface gradient, flow velocity and water depth rasters, respectively. The resulting mesohabitat code (M) uniquely identifies each NMCM mesohabitat category (Table 2). The initial classification yielded 11 mesohabitat categories; two of these are rare or absent in nature according to Borsányi et al. (2004) and were merged with the closest NMCM categories, resulting in nine final mesohabitat types. Merging was based primarily on how the two classes appeared in the Tana River in autumn 2025 and secondarily on their most common proximity in the simulation results. Unlike the field-based NMCM protocol, we did not limit the maximum number of mesohabitat categories across a cross-section; all categories present in the hydraulic outputs were retained. However, the mesohabitat raster was sieved to remove individual habitat patches smaller than 100 m^2. Minimum patch size thresholds (10, 50, 100, 500 and 1000 m^2) were tested to evaluate scale dependency. Sensitivity analysis showed that habitat proportions stabilized at a minimum patch size of approximately 100 m^2. Increasing the threshold beyond 100 m^2 led to loss of tens of thousands of square meters of specific habitat types, whereas smaller thresholds (10 and 50 m^2) retained small, fragmented patches likely representing microhabitat variability rather than ecologically relevant mesohabitat units. Practically, these $< 100\,m^2$ habitat patches were converted to represent the surrounding habitats. Thus, the area of a single mesohabitat unit was at least 100 m^2, but most of the mesohabitat units along the Tana River were much larger than this. Again, a comparison with aerial imagery (National Land Survey of Finland 2015; *Geovekst, 2019; Google Earth, n.d.*) showed that the 100-m^2 threshold corresponded well with the river's hydromorphological structure, and at the same time, we found it ecologically meaningful habitat unit for Atlantic salmons.

A mesohabitat raster was produced for the entire AOI and repeated for all nine discharge scenarios (Table 1), addressing RQ1 by delivering spatially continuous (1-m resolution) mesohabitat maps for the full 53-km reach. The scenarios underpin RQ2 by enabling quantification of seasonal differences in (i) occurrence, (ii) extent and (iii) longitudinal distribution along the river corridor.

Transitions between seasons were encoded at the pixel level as:

$$x = M_1 \times 1000 + M_2 \quad (3)$$

where M_1 and M_2 denote the mesohabitat codes of the earlier and later seasons, respectively. This encoding yielded a six-digit value whose first three digits denote the initial season and last three digits the subsequent season. All spatial analyses, including raster classifications, were conducted in QGIS 3.34.8 using the Raster Calculator.

To complement area-based metrics, mesohabitat diversity was quantified using the Shannon–Weaver index, H′ (Shannon and Weaver 1949):

$$H' = -\sum_{i=1}^{S} p_i \ln(p_i) \quad (4)$$

where S is the number of mesohabitats and p_{i} is the relative proportion of each mesohabitat in the wetted area of the AOI. High H' indicates high mesohabitat diversity, whereas low H' indicates low diversity. The Shannon–Weaver index is widely used in various scientific fields (e.g., ecology and genetics) to examine the diversity and evenness of a selected group. The Shannon–Weaver index has been previously applied to NMCM-based mesohabitat analyses (Casas-Mulet et al. 2014).

2.5 | Habitat Information for Atlantic Salmon

Atlantic salmon were addressed via interpretation of NMCM mesohabitat types based on established ecological knowledge rather than explicit habitat-suitability modelling. No empirical mapping of salmon was performed in this study. Several salmon observation studies have been conducted on the Tana River and its tributaries, and these studies have been carried out on both micro- and meso-scales. We recognized that combining findings from different scales can lead to biases; but in our study the spatial resolution of 1 m xy used in the hydraulic modelling enabled direct linkage to salmon habitat preferences quantified at the microhabitat scale, while the delineation of mesohabitats (minimum area 100 m^2) allowed interpretation at a broader, hydromorphologically meaningful scale. This dual-scale framework supported the use of both micro- and meso-scale observations of salmon habitat use. Previous microhabitat studies provided understanding of depth and velocity preferences, and at the same time, observations at the mesohabitat level showed how fish respond to habitat units that represent broader functional environments rather than isolated point conditions. Because mesohabitats in this study were defined using consistent thresholds (Table 2) applied at the 1-m^2 cell level, the resulting habitat units retain the physical characteristics relevant to microhabitat selection while simultaneously representing spatially coherent patches comparable to mesohabitat classifications used in field-based ecological studies. This hierarchical structure reduces the scale mismatch typically associated with habitat analyses and allows results to be interpreted across both levels.

Typical spawning grounds in autumn are shallow (< 0.5 m) with moderately slow velocity (0.35–0.65 m/s) (Louhi et al. 2008). In the NMCM classification, these corresponded to walks (D), rills (H), shallow glides (B2), shallow rapids (G2) and cascades (F) in terms of depth and flow velocity (Table 2). Cascades (F) have a steep surface gradient and thus are considered less suitable for spawning than the other listed classes.

In the Tana River, juvenile salmon hatch in the spring, emerge from gravel in July and then spend the first years of their lives in the river, most typically 3–5 years (Erkinaro et al. 2019). Previous studies indicated that juveniles preferred slow velocity (< 0.5 m/s) and moderately shallow habitats (0.33–0.74 m) (Mäki-Petäys et al. 2002). In the NMCM classification, these corresponded to pools (C), walks (D) and rills (H) in terms of depth and flow velocity (Table 2). Although the study by Mäki-Petäys et al. (2002) found juveniles in areas deeper than 0.7 m, the study indicated that the juveniles generally preferred shallower areas. For this reason, pools (C) were considered less suitable for salmon juveniles than the other listed classes. Although, based on Metsäniemi et al. (2025) results, juveniles also use deeper areas; salmon fry (age 0+) particularly preferred deep and shallow rapids (G1 and G2), and salmon parr (age > 0+) deep and shallow glides (B1 and B2) as well as deep and shallow rapids in the Tana River.

Based on the above, in the results and discussion sections, we have referred to walks, rills, shallow glides and shallow rapids when discussing mesohabitats suitable for spawning, and to walks, rills, deep and shallow rapids, and deep and shallow glides when discussing mesohabitats suitable for juvenile rearing.

3 | Results

3.1 | Mesohabitat Types

NMCM-based classification (1-m xy resolution) identified nine out of 10 mesohabitat classes along the AOI during the open-channel season. Run mesohabitats were not identified at all in the AOI. Across the nine scenarios, the wetted area and proportional coverage of mesohabitats varied systematically with discharge (Table 3). Deep glides and pools were most common, whereas walks and deep rapids were less frequent (Table 3). High flows expanded deep glides and deep rapids; low flows favoured pools and walks. White water mesohabitats were identified only in the *Alaköngäs* rapid area, and their proportion was the same in all scenarios. Figure 7 illustrates mesohabitats for the Autumn MQ scenario; maps for all scenarios are available at: https://doi.org/10.5281/zenodo.21804136. Broken-surface areas (Figure 8a) became more uniform and less diverse at higher flows, while smoother-surface areas (Figure 8b) changed little across discharges. Longitudinally, mesohabitats formed alternating sequences of broken- and smooth-surface types upstream, with smoother mesohabitats dominating downstream.

2D hydraulic simulations showed that the wetted area within the 53-km AOI averaged 14.3 km^2 in spring (range 12.9–16.6 km^2), 12.1 km^2 in summer (10.9–14.0 km^2) and 11.6 km^2 in autumn (10.2–13.2 km^2), with a 6.4-km^2 difference between Spring MHQ and Autumn MNQ. Mean depth was 2.2 m in spring, 1.4 m in summer and 1.3 m in autumn, ranging from 3.8 m (Spring MHQ) to 1.0 m (Autumn MNQ).

3.2 | Lateral and Longitudinal Distribution of Mesohabitats

Shallow mesohabitats (walks and shallow rapids) were concentrated along riverbanks across seasons. An exception

TABLE 3 | Wetted area, percentage proportion of instream mesohabitats relative to the wetted area, and Shannon–Weaver index (H′) in nine different scenarios. The highest mesohabitat proportion is marked with the darkest blue colour. The first column provides key discharge values calculated from the Onnelansuvanto gauge station time series. Q = discharge; MHQ = mean-high discharge; MQ = mean discharge; MNQ = mean-low discharge. Mesohabitats: A = run; B1 = deep glide; B2 = shallow glide; C = pool; D = walk; E = white water; F = cascade; G1 = deep rapid; G2 = shallow rapid; H = rill.

			Mesohabitats, %										
	Simulated Q m^3/s	Wetted area km^2	A	B1	B2	C	D	E	F	G1	G2	H	H′
Spring MHQ 1191 m^3/s	1188	16.6	0	66	<1	8	2	<1	<1	24	<1	<1	0.93
Spring MQ 407 m^3/s	417	14.3	0	59	<1	19	5	<1	<1	15	1	<1	1.15
Spring MNQ 207 m^3/s	213	12.9	0	51	1	24	11	<1	<1	10	3	<1	1.34
Summer MHQ 349 m^3/s	353	14.0	0	57	1	20	7	<1	<1	13	2	<1	1.22
Summer MQ 167 m^3/s	168	12.1	0	47	1	28	12	<1	<1	9	3	<1	1.36
Summer MNQ 97 m^3/s	97	10.9	0	33	2	35	20	<1	<1	6	4	<1	**1.46**
Autumn MHQ 230 m^3/s	230	13.2	0	52	1	22	11	<1	<1	10	3	<1	1.32
Autumn MQ 130 m^3/s	129	11.6	0	42	2	31	14	<1	<1	7	4	<1	1.41
Autumn MNQ 69 m^3/s	69	10.2	0	23	2	39	27	<1	<1	4	5	<1	1.44

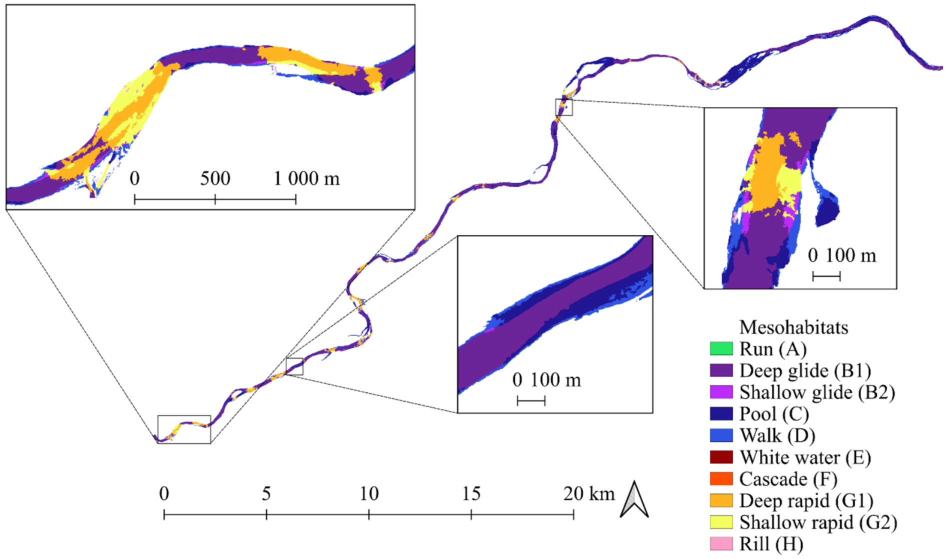

FIGURE 7 | Mesohabitats at Autumn MQ scenario.

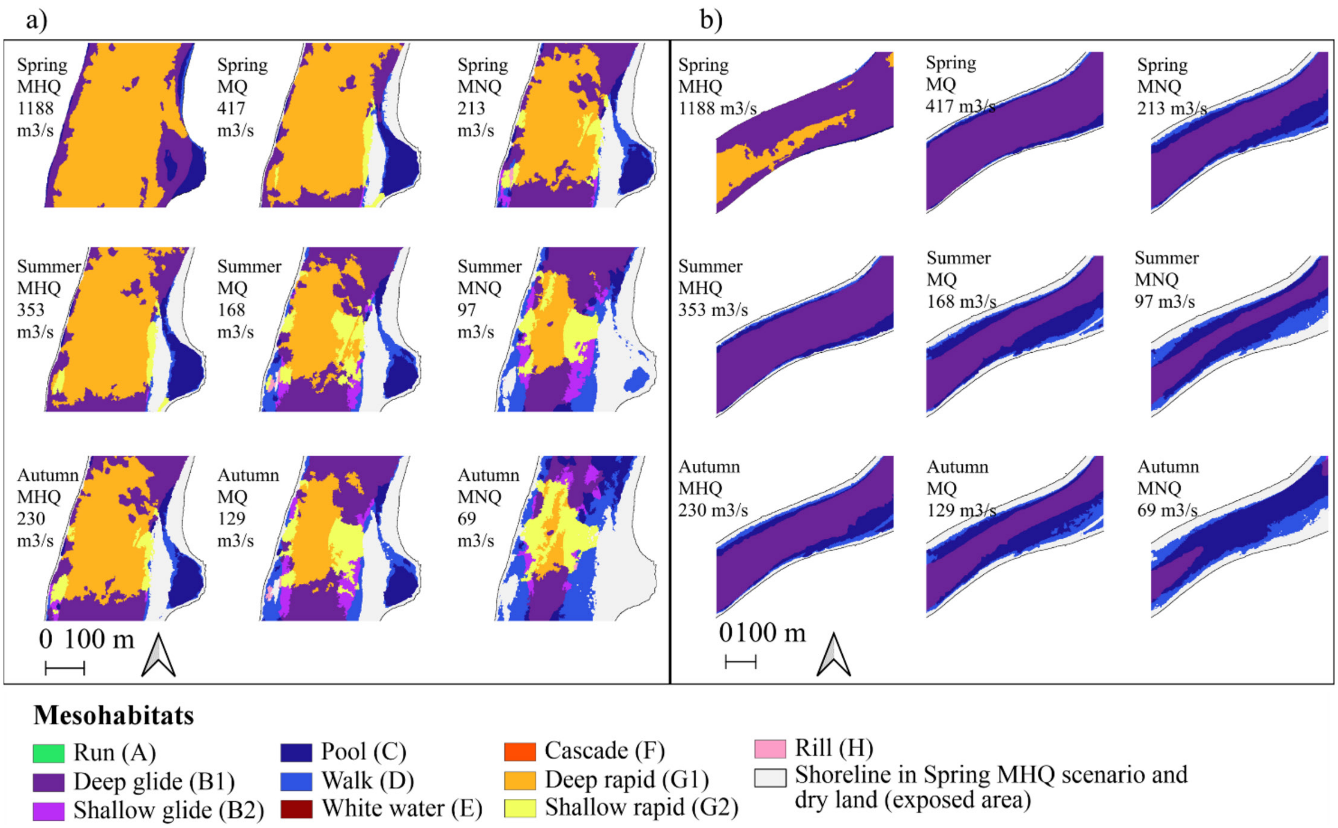

FIGURE 8 | Changes in one area consisting of mesohabitats with (a) broken surface patterns and (b) smoother surface patterns in nine different scenarios. MHQ = mean-high discharge, MQ = mean discharge, MNQ = mean-low discharge.

occurred upstream of *Alaköngäs*, where the midchannel sandbar *Geavgŋoaisáttu* (Figure 9b) supported walk habitats under high flows. At higher discharges (roughly $> 200\,m^3/s$), shallow bank zones (depth < 0.7 m) were typically less than 10 m wide; under lower flows (roughly $< 100\,m^3/s$), they often extended tens of meters. Even at the lowest discharge (Autumn MNQ, $69\,m^3/s$), the thalweg remained > 0.7 m deep throughout the AOI, thus being dominated by deep mesohabitats (deep glides, pools, deep rapids and white waters) in all scenarios. Longitudinally, the upper ~36 km alternated between broken-surface (deep/shallow rapids, cascades, rills and white water) and smoother-surface (deep glides, pools and walks) areas (Figure 9a). The subsequent ~2-km *Alaköngäs* rapid reach was dominated by deep rapids and white waters. Immediately downstream, a ~2-km gravel–sandbar complex (*Bajitjalvi–Boratbovccis–Geavgŋávuolle*, Figure 9c) exhibited high

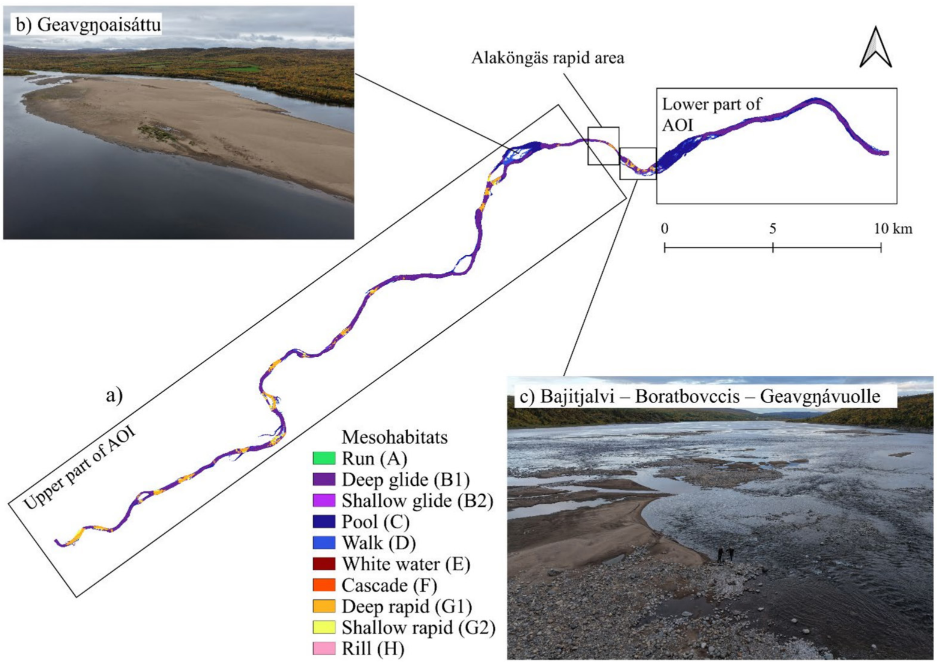

FIGURE 9 | (a) Distribution of mesohabitats in flow direction within the AOI (Spring MNQ situation shown in the figure). (b) Geavgŋoaisáttu in September 2025. At higher flows, the area is completely covered by water. (c) Geavgŋávuolle in September 2025.

mesohabitat diversity, while the final ~13 km was dominated by smoother-surface mesohabitats.

3.3 | Area Distributions of NMCM Classes at Different Flow Rates

Comparisons across five scenarios (Spring MHQ 1188 m^3/s, Spring MQ 417 m^3/s, Summer MQ 168 m^3/s, Autumn MQ 129 m^3/s and Autumn MNQ 69 m^3/s) showed that among NMCM criteria, flow velocity and water depth varied most with discharge (Figure 10). Broken surface patterns declined moderately (≤ 14%) with lower discharge; surface gradient remained practically unchanged. Rapidly flowing areas decreased substantially (up to 60%), and deep areas declined moderately (up to 32%).

3.4 | Variation in Mesohabitats Between and Within Seasons

Between-season contrasts were greater for spring versus summer and spring versus autumn than for summer versus autumn in both proportions (Table 3) and locations (Figure 8) of mesohabitats. Across all seasons, deep glides, pools, walks and deep rapids dominated, with shifting proportions. Spring was characterized by extensive deep glides (51%–66%), whereas summer and autumn alternated between deep glides (23%–57%) and pools (20%–39%). Deep rapids were most frequent in spring (10%–24%) and least in autumn (4%–10%); walks were most common in autumn (11%–27%) and least in spring (2%–11%). Shallow glides, cascades and rills were absent in spring. In the upper AOI, broken-surface areas separated between spring and summer, with smoother mesohabitats forming between them; in the lower AOI, seasonal change was milder, with pools replacing deep glides from spring to summer/autumn. The Shannon–Weaver index (H′) peaked in autumn (1.32–1.44), was slightly lower in summer (1.22–1.46) and lowest in spring (0.93–1.34). Although, Summer MNQ had the highest H′ (1.46), followed by Autumn MNQ (1.44) and Autumn MQ (1.41); Spring MQ (1.15) and Spring MHQ (0.93) were markedly lower.

Within-season variation showed clear high- versus low-flow differences (Table 3). However, the same four key mesohabitats (deep glides, pools, walks and deep rapids) dominated across all seasons and discharges, with only their relative proportions varying. Spring scenarios were most similar in terms of their mesohabitats; autumn scenarios varied most. In spring, deep glides dominated (51%–66%) but declined with decreasing discharge, while pools increased but did not surpass deep glides; deep rapids peaked at Spring MHQ (24%), and walks were scarce (2%) but rose at Spring MNQ (11%). Shallow glides, cascades and rills were absent at Spring MHQ. Deep glides (47%) and pools (28%) also dominated the Summer MQ. Walks accounted for 12%, and deep rapids for 9%. Summer MHQ expanded deep glides (57%) and reduced pools (20%), with walks nearly vanishing except at *Geavgŋoaisáttu* (Figure 9b). Summer MNQ favoured pools (35%), followed by deep glides (33%) and walks (20%). In autumn, MHQ and MQ favoured deep glides (42%–52%); MNQ favoured pools (39%) with diverse broken-surface zones at MQ and narrower channels with sandbars and extensive walks (27%) at MNQ, as deep glides dropped to 23%.

3.5 | Mesohabitat Transition Between Seasons

Figure 11 shows the transition between mesohabitat classes between average spring (Spring MQ) and average summer

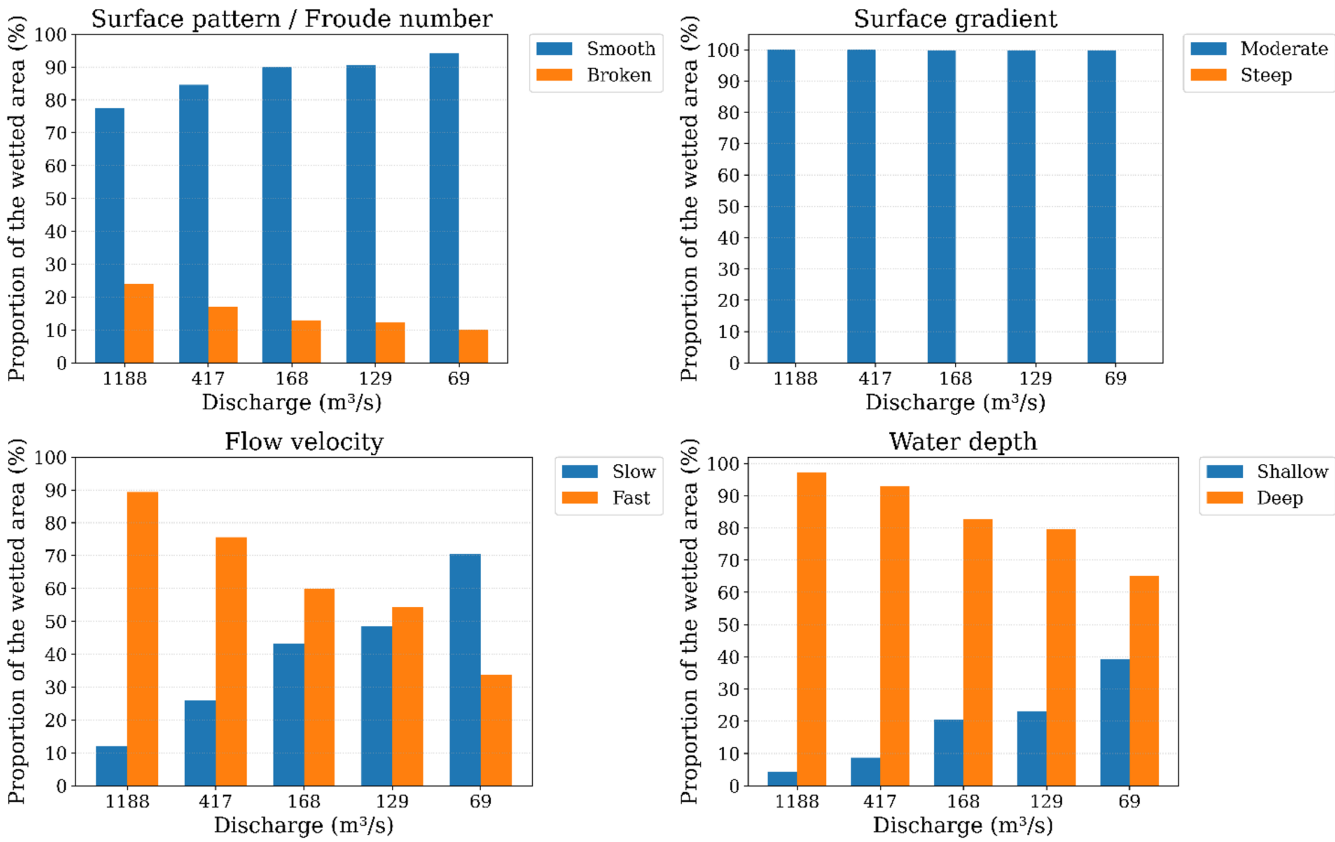

FIGURE 10 | Distribution of wetted area based on NMCM criteria (surface pattern, surface gradient, flow velocity and water depth) in five different discharge scenarios (mentioned under x-axes 1188…69 m^3/s).

(Summer MQ) and between average summer (Summer MQ) and average autumn (Autumn MQ).

From Spring MQ to Summer MQ, shallow spring habitats (shallow glides, walks, cascades, shallow rapids and rills) were largely dry by summer (≥ 80% of their spring area became dry) (Figure 11a). Among deep habitats, pools dried most (23%), followed by white waters (17%). Only three mesohabitats retained at least half of their spring area as the same type: deep glides (60%), pools (58%) and white waters (76%). Walks and rills disappeared totally from their original locations. This did not mean these habitats vanished in summer; they still existed but shifted to different locations than in spring. Spring deep rapids fragmented notably in summer. A small portion of nearly all spring mesohabitats—except walks, white waters and rills—converted to walks in summer. Overall, the transition from spring to summer was characterized by extensive drying and fragmentation of shallow mesohabitats, and substantial reorganization of deep habitats, indicating a major structural shift in mesohabitat configuration.

From Summer MQ to Autumn MQ, changes were minor (Figure 11b). Most habitats remained largely unchanged (57%–89%), except shallow glides and rills. Only 33% of summer shallow glides remained as shallow glides; 58% became walks. Of rills, 17% persisted and 62% dried. A significant proportion (30%–62%) of shallow mesohabitats (walks, cascades and rills) turned into dry land in autumn, while shallow rapids were relatively stable (72% remained shallow rapids). Deep habitats rarely dried (with the exception of 8% of white waters). Most habitats—except white water and deep rapids—partly converted to walks. Only a few mesohabitats converted into shallow glides in autumn (5% of shallow rapids and 2% of deep glides). Similarly, only white waters and deep rapids changed into deep glides in autumn (Figure 11b).

3.6 | Seasonal Variation in Atlantic Salmon-Relevant Mesohabitats

Without explicit habitat-suitability modelling, we report seasonal changes in mesohabitats previously linked to Atlantic salmon spawning and juvenile rearing (see Section 2.5). Three of the four key mesohabitats of AOI—deep glides, walks and deep rapids—can be considered important for Atlantic salmon. Potential spawning habitats (shallow glides, walks, shallow rapids and rills) increased by 124%–770% as discharge decreased (Table 4), peaking in autumn. Deep and fast habitats used by juveniles (deep glides and deep rapids) were most abundant in spring and then declined (28%–81%), remaining slightly more common in summer than autumn. Shallow and slow habitats (walks and rills) and shallow and fast habitats (shallow glides and shallow rapids) preferred by juveniles peaked in autumn and were least common in spring (Table 4).

An important factor regarding salmon habitat use relates to the relative locations of mesohabitats and the combinations of specific types of mesohabitats. For example, it is generally understood that salmon use fast-flowing areas for feeding and slow-flowing areas for resting. In practice, this means that, for example, fast-flowing

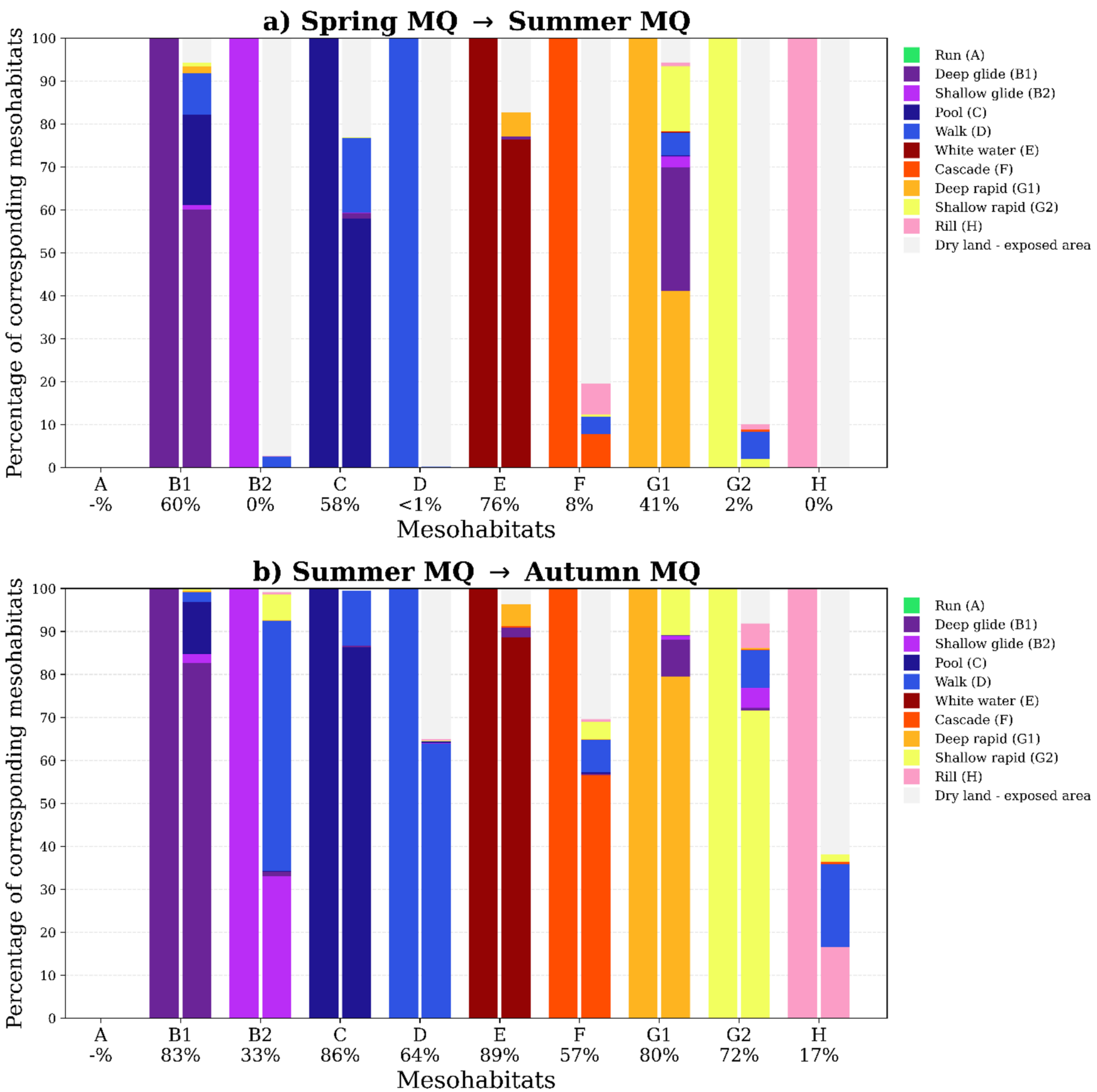

FIGURE 11 | Change in mesohabitat as % of area (a) from the Spring MQ scenario to Summer MQ scenario and (b) from the Summer MQ scenario to Autumn MQ scenario. The percentages on the x-axis indicate how much of the habitat has remained unchanged between the two scenarios. For example, of the habitats classified as type B1 in the Spring MQ scenario, 60% remained type B1 in summer, while 1% shifted to B2, 21% to C, 10% to D, 2% to G1, 1% to G2 and 6% transition to dry land. The information presented in this figure is shown as numerical values in Tables S1 and S2.

glides and rapids combined with slow-flowing walks provide salmon a meaningful environment consisting of two different mesohabitats. Based on our mesohabitat results, the thalweg of the Tana River within the AOI is dominated by deep glides and deep rapids, while the banks are dominated by pools and walks (Figure 8). This pattern became particularly pronounced in the autumn and during lower discharges.

However, even more important factors in terms of salmon mesohabitat use are the availability of food and the presence of predators; unfortunately, the data we had did not allow us to take these biological factors into account.

4 | Discussion

4.1 | Seasonal Dynamics and Diversity of Mesohabitats in the Tana River

Our findings showed that in the near-pristine Tana River, instream mesohabitats shifted markedly across the ice-free period because of strong discharge variability. The mesohabitats were dynamic and seasonally shifting entities rather than static patches, as Maddock (1999) also noted. Based on our results (Table 3), deep glides and pools dominate most of the open-water season (23%–66% and 8%–39% of AOIs wetted area,

TABLE 4 | Areas (km²) of mesohabitats that have been assessed as important for Atlantic salmon spawning and rearing, in different scenarios. The upper part of the table shows which mesohabitats are assessed as important for spawning (o) and juvenile salmon (x). The highest value in each column is marked with the darkest blue colour.

	Deep glide B1	Shallow glide B2	Walk D	Deep rapid G1	Shallow rapid G2	Rill H
Spawning (Louhi et al. 2008)		o	o		o	o
Fry, 0+ (Metsäniemi et al. 2025)				x	x	
Parr, >0+ (Metsäniemi et al. 2025)	x	x		x	x	
Juveniles (all ages) (Mäki-Petäys et al. 2002)			x			x
Spring MHQ	10.9	0.01	0.4	3.9	0.0	0.00
Spring MQ	8.4	0.08	0.6	2.2	0.2	0.01
Spring MNQ	6.6	0.13	1.4	1.2	0.4	0.04
Summer MHQ	7.9	0.13	0.9	1.9	0.3	0.01
Summer MQ	5.7	0.14	1.4	1.0	0.4	0.03
Summer MNQ	3.6	0.23	2.2	0.6	0.4	0.04
Autumn MHQ	6.9	0.13	1.4	1.3	0.4	0.03
Autumn MQ	4.8	0.20	1.6	0.9	0.4	0.03
Autumn MNQ	2.3	0.23	2.8	0.4	0.5	0.04

respectively). Metsäniemi et al. (2025) likewise reported a high proportion of deep glides (19.7%) along a 200-km reach of the Tana River in August–September 2014, exceeded only by sandy runs (66.6%). It should be noted that we studied a 53-km long section of the Tana River, which is clearly more rapids-prone than the rest of the river. Our analyses revealed that spring floods favour deep glides, deep rapids and pools while shallow habitats nearly vanish; by contrast, summer–autumn low flows expand shallow margins and increase walks (Table 3, Figure 8). Similar dynamic patterns have been observed also in other rivers (O'Sullivan et al. 2020).

Moreover, our class transition analysis indicates that the sharpest mesohabitat reorganization occurs from spring to summer (Figure 11); summer and autumn were more alike, indicating that the spring flood described by Dankers (2002) has a radical impact on mesohabitats. The Tana River is typically ice-covered from early November to early May without freezing to the bed; ice breakup is followed by a spring flood. Between 1959 and 2024, mean spring discharge at O*nnelansuvanto* was 407 m^3/s, ~3 times the annual mean (139 m^3/s), after which flow declines toward autumn and drops to ~20–50 m^3/s in winter (Figure 3). Our results also align with gravel-bed and cold-region river studies showing that snowmelt floods are the dominant drivers of hydraulic and geomorphic restructuring; subsequent lower-flow periods tend to modify rather than fundamentally reorganize habitat mosaics (Driscoll and Hauer 2019; Irannezhad et al. 2022). During flood recession, wetted area contracts and spring–summer transitions were characterized by widespread drying and relocation of shallow mesohabitats; shallow classes are therefore among the most discharge-sensitive types, which have been documented also in other river systems (Driscoll and Hauer 2019; Mortensen et al. 2024). Conversely, once deep glides, pools and other main-channel habitats are established after spring recession, their extent and configuration remain relatively stable under moderate summer–autumn variability (Figure 11); a similar phenomenon has also been reported by Driscoll and Hauer (2019). Together, these patterns underscore the dominant role of spring floods in restructuring mesohabitat configuration along the study site, supporting the broader conceptual understanding that morphology provides the template for potential habitat diversity, whereas seasonally predictable high-magnitude floods determine which mesohabitats are expressed at a given time (Wallis et al. 2012).

It is important to note that in the subarctic region, interseasonal precipitation correlations are low (a rainy spring does not imply a rainy summer/autumn), yet river discharge correlates with precipitation, particularly in summer and autumn (Rawlins et al. 2009). Consequently, within a single ice-free period, sequences such as Spring MHQ → Summer MNQ → Autumn MHQ are plausible, producing substantial mesohabitat variability in discharge-sensitive systems.

Inspection of the NMCM criteria showed discharge chiefly alters velocity and depth, with limited change in surface pattern and surface gradient (Figure 10). The water surface gradient is primarily set by riverbed slope, although discharge—especially flood peaks—can have a minor effect (Bauer-Gottwein et al. 2024). Because our DTM (and thus riverbed slope) was held constant across scenarios, we did not observe any gradient differences among discharges. Surface pattern arises from discharge interacting with channel morphology, including velocity, bed roughness and turbulence (Muraro et al. 2021), so discharge changes alone should exert a modest influence on surface pattern—as was the case in our results (Figure 10). Wind-generated capillary-gravity waves can also affect surface pattern (Muraro et al. 2021), but wind was not included in our 2D hydraulic simulations.

In our results, the Shannon–Weaver index was highest under Summer MNQ and lowest under Spring MHQ (Table 3), aligning with findings that lower flows increase habitat diversity (Casas-Mulet et al. 2014). In our study, high flows homogenized especially the broken-surface pattern zones, reducing mesohabitat diversity. Alcaraz-Hernández et al. (2011) similarly observed greater pool heterogeneity in streams with lower mean discharge than in higher-discharge systems.

4.2 | Implication of Seasonal Mesohabitat Dynamics for Atlantic Salmon

The seasonal mesohabitat variation in the Tana River is likely important for certain life stages of Atlantic salmon. Autumn offers shallow, moderately slow habitats (walks, rills, shallow glides and shallow rapids; Tables 3 and 4) that are characterized by shallow depths and moderate velocities, which correspond to microhabitat conditions preferred by spawning salmon (Louhi et al. 2008) and juveniles (Mäki-Petäys et al. 2002). In spring and summer, when fry emerge, many of these habitats transform into deeper, faster mesohabitats (deep glides, deep rapids; Tables 3 and 4) that Metsäniemi et al. (2025) identified as important for juvenile salmon in the Tana River. Our results indicated that deep glides are prominent in spring and summer, aiding newly emerged fry, while the increased availability of walks in autumn corresponds to hydraulic conditions suitable for spawning reported at the microhabitat scale. This dynamic may also partly explain the Tana River's high ecological value for Atlantic salmon.

Although we did not model future discharge scenarios explicitly, the observed sensitivity of mesohabitat structure to seasonal flow variation provided insight into potential impacts of projected hydrological change. Climate change is projected to intensify autumn rainfall in the Tana River basin (Moradian et al. 2023), potentially making autumn hydrology more summer-like. Two concerns arise for salmon. First, our results indicated that shallow mesohabitats decrease significantly as discharge increases (Table 3). Autumn high flows can yield mesohabitat distributions resembling spring low-flow states, with the share of walks declining by up to 12% compared with average autumn, and other shallow mesohabitats scarce (Table 3). Second, reduced seasonal variability itself may be detrimental. If a naturally dynamic environment becomes less dynamic, organisms must adapt. If shallow spawning habitats become unavailable or rare, the river's potential for salmon reproduction may decrease. This is concerning, given the already weak Tana River salmon stock (Anon 2026). Follow-up studies should examine how climate change affects mesohabitat dynamics.

We also note that substrate type, a key salmon habitat attribute at multiple life stages (Mäki-Petäys et al. 2002; Louhi et al. 2008), was not mapped in this study. Substrate is part of NMCM, adding another level to classification (Borsányi et al. 2004). However, the longitudinal gradient and flow velocity of a river indicate the substrate type, particularly the grain size, because, according to Lane's equilibrium (Lane 1954), the erosion and transport capacity of a river increase as the discharge and longitudinal gradient increase; in other words, a fast and steep current can move coarser material than a slow and moderate one. In our study, this means that in mesohabitats with moderate gradient and slow flow velocity (pools, walks and rills), we can assume that the substrate median grain size (D50) is finer than in mesohabitats with steep gradient and fast flow velocity. However, it would be beneficial to investigate substrate identification as part of our approach in the future.

4.3 | Methodological Considerations, Uncertainties and Applicability

We combined multispectral ALS, 2D hydraulic modelling and NMCM to create a methodological approach that enabled us to examine ecological phenomena that previously could not be studied on the Tana River due to limitations in high-resolution data availability with large area coverage, and/or due to discharge variation. The novelty lies less in method development than in what the integrated method makes observable. ALS and 2D modelling together provided broad coverage and fine resolution for simulating NMCM hydraulic criteria. Based on previous studies in other rivers (e.g., Marchamalo et al. 2007; Tonina et al. 2020), conducting 1-m resolution mapping over 53 km and nine discharge scenarios by field-based methods would have been prohibitively time-consuming. Moreover, a single ALS dataset supported both geometry construction and hydraulic model calibration, addressing two major challenges for long and non-wadable rivers. In the Tana River, the thalweg is too deep to wade even at low flows, and strong currents at the *Alaköngäs* rapids preclude field-based delineation.

Optical bathymetric methods could also produce DTMs, but ALS has a key advantage: direct elevation measurement without separate reference data. Optical approaches require in-water depth calibration and are sensitive to factors such as surface roughness, bottom reflectance variability, illumination and deep areas (Kasvi et al. 2019). Challenges intensify on wide rivers, where multiple flight lines are needed to ensure resolution and coverage; Central portions can lack reference points because images capture only water, complicating accurate georeferencing (Román et al. 2024). ALS has constraints too (see 2.2.1 Multispectral Airborne Laser Scanning). Neither ALS nor optical methods resolve undercut banks; while absent in our AOI, they occur in subarctic rivers. ALS data also age: Strong spring floods (Dankers 2002) and dynamic ice breakup (Beltaos and Burrell 2021) can reshape the bed, so maintaining up-to-date DTMs would require periodic, ideally postflood, ALS acquisitions.

2D modelling also has limitations, particularly its dependence on defined boundary conditions for discharge. Models can be built with estimated discharges, but with larger uncertainty. Obviously, expanding the scenario set requires more measurements or reliable estimates. The Tana River is advantageous because daily discharge is recorded at multiple gauges over decades. However, tributaries posed difficulties; 18 larger and many smaller tributaries enter the Tana River, most ungauged.

Inflow boundary specification strongly affects 2D results (Brunner 2025). We addressed this by limiting the study between *Utsjoki* and *Polmak*, with three larger tributaries, with the Utsjoki River gauged daily. With gauges at the AOI's upstream and downstream boundaries, we computed the combined ungauged inflow as the intergauge difference and found it small enough to conclude that, aside from the Utsjoki River, tributary inflows did not essentially affect results.

Classifying surface pattern using only the Froude number simplified and accelerated processing but introduces uncertainty because distinct velocity–depth combinations can yield similar Froude values (Clifford et al. 2006). Interpretation of deep glide versus deep rapid, shallow glide versus shallow rapid, run versus white water and walk versus rill should therefore consider that these pairs differ only by surface pattern. A richer predictor set—for example, velocity + depth + Froude + stream power + discharge as in Casas-Mulet et al. (2014)—could improve surface-pattern rasters and mesohabitat maps, albeit at the cost of workflow complexity. In our results, however, discharge-driven changes were largest for velocity and depth, while surface-pattern changes were modest (Figure 10). From an Atlantic salmon perspective, whether a mesohabitat is a deep glide or a deep rapid may be less consequential than whether it is a deep glide versus a walk, supporting the pragmatic use of Froude number here.

A minor challenge arose because parameterization via the hydraulic model yielded 11 mesohabitat classes, whereas the initial NMCM lists 10 (Borsányi et al. 2004). Although Borsányi et al. (2004) recognized 16 theoretical classes, six were removed as extremely rare or absent in nature. We found small amounts (0.005% of wetted area on average) of classes omitted from the NMCM and merged them into walk (D) and cascade (F) categories based on the most frequent adjacency in our results and September 2025 field appearance in the Tana River. When interpreting results, it is also worth noting that simulated scenarios were tied to real dates representative of average seasonal conditions to increase hydraulic model reliability and enable validation of each scenario against observed stages; as a result, scenarios did not match statistical discharge metrics (MQ, MHQ and MNQ) in every respect (Table 3). However, this approach offered robust, scenario-specific validation using available water-level observations. Our approach has limitations also at *Alaköngäs*, where turbulence hinders laser penetration; we therefore assumed larger bed-elevation errors there. Because DTMs are a major uncertainty source in 2D hydraulic modeling (Hauer et al. 2009; Wyrick et al. 2014), mesohabitat results in the *Alaköngäs* warrant caution. Nonetheless, *Alaköngäs* is relatively short (~2 km), and our maps indicate that it is dominated by deep rapids and white water, a combination that is not among the most significant habitats for Atlantic salmon in the study area.

Overall, the approach is transferable to rivers of various sizes, provided water turbidity, turbulence and bank structure permit green-laser penetration and discharge can be measured or estimated reliably. It is well-suited for modeling prospective flows to support climate impact assessments. Nevertheless, mesohabitat maps alone do not directly indicate organism occurrence because ecological processes and biological behavior are not represented (Armstrong et al. 2003; Sillero 2011).

5 | Conclusions

This study demonstrates the potential of integrating multispectral ALS data, 2D hydraulic modelling, NMCM and long-term discharge series to analyse the dynamics of instream mesohabitats at high spatial and temporal resolution, providing a new observational level for ecohydrological research.

The following observed patterns may also apply to other large, near-pristine rivers of the Northern Hemisphere with similar hydrological regimes:

- Seasonal discharge variation alters mainly water depth and velocity, resulting in substantial changes in mesohabitat extent, diversity and spatial distribution.
- The strongest habitat reorganization occurs between spring and summer, when recession of the spring snowmelt flood transformed extensive deep-water habitats into a more diverse mosaic of mesohabitats. Summer-to-autumn changes are considerably smaller.
- Spring high discharges favor deep glides and deep rapids, whereas declining summer and autumn discharges increase the extent of pools, walks and other shallow habitats.
- Lower discharges appear to support higher mesohabitat diversity.
- Mesohabitat change involves both shifts in habitat proportions and relocation of habitats in space, demonstrating that mesohabitats are dynamic entities rather than static patches. Changes can occur both between seasons and within seasons.
- The ecological significance of the seasonal reorganization of mesohabitats is that it aligns with the needs of Atlantic salmon. Shallow mesohabitats, which are especially important for Atlantic salmon spawning, were most abundant in the autumn, whereas the variation between deeper and shallower mesohabitat types between spring and summer may benefit juvenile salmon, which have been found to use not only shallow habitats but also deeper ones. Mesohabitat seasonal variation may help maintain suitable habitat conditions for salmon at different life stages during their freshwater residence.

The continuous mapping of mesohabitats across space and multiple discharges provides quantitative information on the dynamic environment in which Atlantic salmon spawn and spend their early years. The approach is applicable across a wide range of river conditions, including deep and nonwadable channels, although its performance depends on water clarity, laser penetration possibilities and discharge data availability. The lack of substrate information represents a key limitation and should be addressed in future developments of the framework. Moreover, future research should integrate climate change–driven hydrological scenarios into the hydraulic modelling framework to enable more robust conclusions.

Overall, the results highlight the dynamic and seasonally variable nature of instream mesohabitats and emphasize the importance of incorporating temporal variability into ecohydrological analyses. Expanding the use of integrated remote sensing and hydraulic modelling approaches offers significant potential for improving process understanding and supporting river management under changing environmental conditions.

Author Contributions

Emmy Kärkkäinen: conceptualization, methodology, data curation, formal analyses, project administration, visualization, interpretation, writing – original draft, writing – review and editing. **Ville Kankare:** conceptualization, writing – review and editing, supervision. **Jaakko Erkinaro:** writing – review and editing, supervision. **Mikel Calle:** data acquisition. **Harri Kaartinen:** data acquisition, data curation, writing – review and editing, resources. **Petteri Alho:** conceptualization, writing – review and editing, supervision, resources, project administration, funding acquisition.

Acknowledgements

This research is a part of the Ministry of Education and Culture's Doctoral Education Pilot under Decision No. VN/3137/2024-OKM-6 (Digital Waters (DIWA) Doctoral Education Pilot in Finland related to the DIWA Flagship (Decision No. 359247) funded by the Research Council of Finland's Flagship Programme. European Union—The Next Generation EU recovery instrument (RRF) through the Research Council of Finland supported multispectral ALS data acquisition via the project Green-Digi-Basin (Decision Nos. 347701 and 347702). We want to thank current and past members of the Fluvial and Coastal Research Group who participated in the fieldwork, and two reviewers for their excellent comments, which helped improve this article. Open access publishing facilitated by Turun yliopisto, as part of the Wiley - FinELib agreement.

Funding

This work was supported by the Research Council of Finland (359247, 347701 and 347702).

Disclosure

The authors acknowledge the use of Microsoft Copilot to support creation of the abstract and to suggest reorganization of the Results and Discussion sections for clarity and flow. DeepL was used to translate individual phrases and sentences from Finnish to English. All AI-generated suggestions were reviewed, revised and approved by the authors, who take full responsibility for the accuracy and integrity of the work.

Data Availability Statement

Derived raster products (mesohabitat maps) will be made available upon reasonable request. The original laser scanning data or aerial photographs cannot be shared under the terms of the data provider. All mesohabitat maps can be found in the online repository: https://doi.org/10.5281/zenodo.21804136.

Discharge and water level records from the *Onnelansuvanto* and *Patoniva* gauge stations are available at: https://wwwp2.ymparisto.fi/scripts/kirjaudu.asp. Discharge and water level records from the *Polmak nye* gauge station are available at: https://sildre.nve.no/map.

References

Alcaraz-Hernández, J. D., F. Martínez-Capel, M. Peredo Parada, and A. B. Hernández-Mascarell. 2011. "Mesohabitat Heterogeneity in Four Mediterranean Streams of the Jucar River Basin (Eastern Spain)." *Limnetica* 30, no. 2: 363–378. https://doi.org/10.23818/limn.30.26.

Anon. 2026. *Status of the Tana/Teno River Salmon Populations in 2025: Report From the Tana/Teno Monitoring and Research Group*. Tana Monitoring and Research Group. Available at: https://jukuri.luke.fi/handle/11111/103692 Accessed: January 29, 2026.

Armstrong, J. D., P. S. Kemp, G. J. A. Kennedy, M. Ladle, and N. J. Milner. 2003. "Habitat Requirements of Atlantic Salmon and Brown Trout in Rivers and Streams." *Fisheries Research* 62, no. 2: 143–170. https://doi.org/10.1016/S0165-7836(02)00160-1.

Bakuła, K. 2015. "Multispectral Airborne Laser Scanning - A New Trend in the Development of Lidar Technology." *Archiwum Fotogrametrii, Kartografii i Teledetekcji* 27: 25–44. https://doi.org/10.14681/afkit.2015.002.

Bauer-Gottwein, P., L. Christoffersen, A. Musaeus, M. C. Frías, and K. Nielsen. 2024. "Hydraulics of Time-Variable Water Surface Slope in Rivers Observed by Satellite Altimetry." *Remote Sensing* 16, no. 21: 4010. https://doi.org/10.3390/rs16214010.

Baumgartner, K. 2020. "Analyse und Evaluierung der praktischen Anwendung von topo-bathymetrischen LiDAR Daten in alpinen Gewässern: Identifizierung morphologischer Strukturen, Erkenntnisse aus der numerischen Strömungs- und Geschiebetransportsimulation." Doctoral Thesis, Leopold-Franzens-Universität Innsbruck, Fakultät fur Technische Wissenschaften. Accessed August 21, 2025. http://ulb-dok.uibk.ac.at/ulbtirolhs/5672816.

Beltaos, S., and B. C. Burrell. 2021. "Effects of River-Ice Breakup on Sediment Transport and Implications to Stream Environments: A Review." *Water* 13, no. 18: 2541. https://doi.org/10.3390/w13182541.

Bisson, P. A., J. L. Nielsen, R. A. Palmason, and L. E. Grove. 1982. "A System of Naming Habitat Types in Small Streams, with Examples of Habitat Utilization by Salmonids During Low Streamflow." In *Acquisition and Utilization of Aquatic Habitat Inventory Information*, edited by N. B. Armantrout, 62–73. American Fisheries Society.

Borsányi, P., K. Alfredsen, A. Harby, O. Ugedal, and C. Kraxner. 2004. "A Meso-Scale Habitat Classification Method for Production Modelling of Atlantic Salmon in Norway." *Hydroecologie Appliquee* 14: 119–138. https://doi.org/10.1051/hydro:2004008.

Bovee, K. D. 1986. *Development and Evaluation of Habitat Suitability Criteria for Use in the Instream Flow Incremental Methodology*. FWS/OBS-86/7. USDI Fish and Wildlife Service. https://pubs.usgs.gov/publication/70121265 Accessed: November 17, 2025.

Brunner, G. W. 2025. *HEC-RAS River Analysis System. HEC-RAS 2D User's Manual*. Version 6.6 ed. Hydrologic Engineering Center.

Burgazzi, G., P. Vezza, G. Negro, et al. 2021. "Effect of Microhabitats, Mesohabitats and Spatial Position on Macroinvertebrate Communities of a Braided River." *Journal of Ecohydraulics* 6, no. 2: 95–104. https://doi.org/10.1080/24705357.2021.1938254.

Casas-Mulet, R., K. Alfredsen, and Å. Killingtveit. 2014. "Modelling of Environmental Flow Options for Optimal Atlantic Salmon, Salmo Salar, Embryo Survival During Hydropeaking." *Fisheries Management and Ecology* 21, no. 6: 480–490. https://doi.org/10.1111/fme.12097.

Casulli, V. 2008. "A High-Resolution Wetting and Drying Algorithm for Free-Surface Hydrodynamics." *International Journal for Numerical Methods in Fluids* 60, no. 4: 391–408. https://doi.org/10.1002/fld.1896.

Clifford, N. J., O. P. Harmar, G. Harvey, and G. E. Petts. 2006. "Physical Habitat, Eco-Hydraulics and River Design: A Review and re-Evaluation of Some Popular Concepts and Methods." *Aquatic Conservation: Marine and Freshwater Ecosystems* 16, no. 4: 389–408. https://doi.org/10.1002/aqc.736.

Collinson, J. D. 1970. "Bedforms of the Tana River, Norway." *Geografiska Annaler: Series A, Physical Geography* 52, no. 1: 31–56. https://doi.org/10.1080/04353676.1970.11879807.

Dankers, R. 2002. *Sub-Arctic Hydrology and Climate Change: A Case Study of the Tana River Basin in Northern Fennoscandia*. Doctoral

Thesis. Universiteit Utrecht, Faculteit Ruimtelijke Wetenschappen Universiteit Utrecht.

Driscoll, K. P., and F. R. Hauer. 2019. "Seasonal Flooding Affects Habitat and Landscape Dynamics of a Gravel-Bed River Floodplain." *Freshwater Science* 38, no. 3: 38. https://doi.org/10.1086/704826.

Eisner, A., C. Young, M. Schneider, and I. Kopecki. 2005. "MesoCASiMiR – New Mapping Method and Comparison with Other Current Approaches." In *COST 626 European Aquatic Modelling Network: Proceedings from the Final Meeting in Silkeborg, Denmark*, edited by A. Harby, M. Baptist, H. Duel, M. J. Dunbar, P. L. M. Goethals, A. Huusko, A. Ibbotson, H. Mader, M. L. Pedersen, S. Schmutz, and M. Schneider, 397. COST Office.

Elbashir, M. A. O. 2019. *2D Hydraulic Modelling of a Braided River System Using Aerial Imagery for Water Depth Mapping: The Wairau River, New Zealand*. Master's Thesis. Technische Universität Dresden, Faculty of Environmental Sciences Department of Hydro Sciences.

Entwistle, N., G. Heritage, and D. Milan. 2019. "Ecohydraulic Modelling of Anabranching Rivers." *River Research and Applications* 35, no. 4: 353–364. https://doi.org/10.1002/rra.3413.

Erkinaro, J., Y. Czorlich, P. Orell, et al. 2019. "Life History Variation Across Four Decades in a Diverse Population Complex of Atlantic Salmon in a Large Subarctic River." *Canadian Journal of Fisheries and Aquatic Sciences* 76, no. 1: 42–55. https://doi.org/10.1139/cjfas-2017-0343.

Farò, D., K. Baumgartner, P. Vezza, and G. Zolezzi. 2022. "A Novel Unsupervised Method for Assessing Mesoscale River Habitat Structure and Suitability From 2D Hydraulic Models in Gravel-Bed Rivers." *Ecohydrology* 15, no. 7: e2452. https://doi.org/10.1002/eco.2452.

Farò, D., T. S. Parra, K. Baumgartner, A. Andreoli, P. Vezza, and G. Zolezzi. 2025. "An Integrated Framework for the Assessment of Meso-Scale Physical Habitats in Gravel-Bed Rivers Using Remote Sensing and 2D Hydraulic Modeling." *WIREs Water* 12, no. 3: e70027. https://doi.org/10.1002/wat2.70027.

Fausch, K. D., C. E. Torgersen, C. V. Baxter, and H. W. Li. 2002. "Landscapes to Riverscapes: Bridging the Gap Between Research and Conservation of Stream Fishes." *Bioscience* 52, no. 6: 483. https://doi.org/10.1641/0006-3568(2002)052%5B0483:ltrbtg%5D2.0.co;2.

Fernandez-Diaz, J., W. Carter, C. Glennie, et al. 2016. "Capability Assessment and Performance Metrics for the Titan Multispectral Mapping Lidar." *Remote Sensing* 8, no. 11: 936. https://doi.org/10.3390/rs8110936.

Frissell, C. A., W. J. Liss, C. E. Warren, and M. D. Hurley. 1986. "A Hierarchical Framework for Stream Habitat Classification: Viewing Streams in a Watershed Context." *Environmental Management* 10, no. 2: 199–214. https://doi.org/10.1007/BF01867358.

Geovekst. 2019. "Orthophoto [Map]." Tana 2019. https://www.norgeibilder.no.

Gibson, S. A., and G. B. Pasternack. 2015. "Selecting Between One-Dimensional and Two-Dimensional Hydrodynamic Models for Ecohydraulic Analysis: Comparing 1D and 2D Ecohydraulic Models." *River Research and Applications* 32, no. 6: 1365–1381. https://doi.org/10.1002/rra.2972.

Glennie, C. L., W. E. Carter, R. L. Shrestha, and W. E. Dietrich. 2013. "Geodetic Imaging With Airborne LiDAR: The Earth's Surface Revealed." *Reports on Progress in Physics* 76, no. 8: 086801. https://doi.org/10.1088/0034-4885/76/8/086801.

Google Earth V 10.112.66.1. n.d. "Tana River, Finland/Norway. 68–70°N, 25–27°E, Eye alt 85 km. Maxar Technologies, Airbus, CNES/Airbus, Landsat/Copernicus." The Imagery Consists of Satellite and Aerial Data Acquired Over Multiple Years. Retrieved June 10, 2026 Available at: https://earth.google.com/.

Hauer, C., G. Mandlburger, and H. Habersack. 2009. "Hydraulically Related Hydro-Morphological Units: Description Based on a New Conceptual Mesohabitat Evaluation Model (MEM) Using LiDAR Data as Geometric Input." *River Research and Applications* 25, no. 1: 29–47. https://doi.org/10.1002/rra.1083.

Hauer, C., B. Schober, and H. Habersack. 2013. "Impact Analysis of River Morphology and Roughness Variability on Hydropeaking Based on Numerical Modelling." *Hydrological Processes* 27, no. 15: 2209–2224. https://doi.org/10.1002/hyp.9519.

Hauer, C., G. Unfer, M. Tritthart, E. Formann, and H. Habersack. 2011. "Variability of Mesohabitat Characteristics in Riffle-Pool Reaches: Testing an Integrative Evaluation Concept (FGC) for MEM-Application." *River Research and Applications* 27, no. 4: 403–430. https://doi.org/10.1002/rra.1357.

Hiedanpää, J., J. Saijets, P. Jounela, M. Jokinen, and S. Sarkki. 2020. "Beliefs in Conflict: The Management of Teno Atlantic Salmon in the Sámi Homeland in Finland." *Environmental Management* 66, no. 6: 1039–1058. https://doi.org/10.1007/s00267-020-01374-6.

Hitchman, S. M., M. E. a. Mather, and J. M. Smith. 2024. "Empirical Assessments of the Type and Strength of Stream Fish Habitat Associations Can Advance Understanding of Functional Diversity and Promote Effective Conservation." *Diversity* 16, no. 12: 722. https://doi.org/10.3390/d16120722.

Hugue, F., M. Lapointe, B. C. Eaton, and A. Lepoutre. 2016. "Satellite-Based Remote Sensing of Running Water Habitats at Large Riverscape Scales: Tools to Analyze Habitat Heterogeneity for River Ecosystem Management." *Geomorphology* 253: 353–369. https://doi.org/10.1016/j.geomorph.2015.10.025.

Irannezhad, M., S. Ahmadian, A. Sadeqi, M. Minaei, B. Ahmadi, and H. Marttila. 2022. "Peak Spring Flood Discharge Magnitude and Timing in Natural Rivers Across Northern Finland: Long-Term Variability, Trends, and Links to Climate Teleconnections." *Water* 14, no. 8: 1–15. https://doi.org/10.3390/w14081312.

Jowett, I. G. 1993. "A Method for Objectively Identifying Pool, Run, and Riffle Habitats From Physical Measurements." *New Zealand Journal of Marine and Freshwater Research* 27, no. 2: 241–248. https://doi.org/10.1080/00288330.1993.9516563.

Jowett, I. G., and M. J. Duncan. 2012. "Effectiveness of 1D and 2D Hydraulic Models for Instream Habitat Analysis in a Braided River." *Ecological Engineering* 48: 92–100. https://doi.org/10.1016/j.ecoleng.2011.06.036.

Kasvi, E., J. Salmela, E. Lotsari, T. Kumpula, and S. N. Lane. 2019. "Comparison of Remote Sensing Based Approaches for Mapping Bathymetry of Shallow, Clear Water Rivers." *Geomorphology* 333: 180–197. https://doi.org/10.1016/j.geomorph.2019.02.017.

Kottek, M., J. Grieser, C. Beck, B. Rudolf, and F. Rubel. 2006. "World Map of the Köppen-Geiger Climate Classification Updated." *Meteorologische Zeitschrift* 15, no. 3: 259–263. https://doi.org/10.1127/0941-2948/2006/0130.

Kuiper, S. D., N. C. Coops, S. G. Hinch, and J. C. White. 2023. "Advances in Remote Sensing of Freshwater Fish Habitat: A Systematic Review to Identify Current Approaches, Strengths and Challenges." *Fish and Fisheries* 24, no. 5: 829–847. https://doi.org/10.1111/faf.12772.

Lamouroux, N., C. Hauer, M. J. Stewardson, and N. L. R. Poff. 2017. "Physical Habitat Modeling and Ecohydrological Tools." In *Water for the Environment*, 265–285. Elsevier. https://doi.org/10.1016/B978-0-12-803907-6.00013-9.

Lane, E. W. 1954. *The Importance of Fluvial Morphology in Hydraulic Engineering, Hydraulic Laboratory Report no. 372*. United States Department of the Interior, Bureau of Reclamation. https://semspub.epa.gov/work/01/554355.pdf.

Legleiter, C. J., and L. R. Harrison. 2019. "Remote Sensing of River Bathymetry: Evaluating a Range of Sensors, Platforms, and Algorithms on the Upper Sacramento River, California, USA." *Water Resources Research* 55, no. 3: 2142–2169. https://doi.org/10.1029/2018WR023586.

Linnansaari, T., A. Keskinen, A. Romakkaniemi, J. Erkinaro, and P. Orell. 2010. "Deep Habitats Are Important for Juvenile Atlantic Salmon *Salmo Salar* L. in Large Rivers." *Ecology of Freshwater Fish* 19, no. 4: 618–626. https://doi.org/10.1111/j.1600-0633.2010.00443.x.

Louhi, P., A. Mäki-Petäys, and J. Erkinaro. 2008. "Spawning Habitat of Atlantic Salmon and Brown Trout: General Criteria and Intragravel Factors." *River Research and Applications* 24, no. 3: 330–339. https://doi.org/10.1002/rra.1072.

Maddock, I. 1999. "The Importance of Physical Habitat Assessment for Evaluating River Health." *Freshwater Biology* 41, no. 2: 373–391. https://doi.org/10.1046/j.1365-2427.1999.00437.x.

Mäki-Petäys, A., A. Huusko, J. Erkinaro, and T. Muotka. 2002. "Transferability of Habitat Suitability Criteria of Juvenile Atlantic Salmon (*Salmo Salar*)." *Canadian Journal of Fisheries and Aquatic Sciences* 59, no. 2: 218–228. https://doi.org/10.1139/f01-209.

Mandlburger, G. 2025. "Airborne Lidar, A Tutorial for 2025, Part III: Bathymetric Lidar." *LIDAR Magazine* 15, no. 2: 1–11. Accessed February 5, 2026. https://lidarmag.com/wp-content/uploads/PDF/LIDARMagazine_Mandlburger-AirborneLidarPart3_Spring2025.pdf.

Mandlburger, G., C. Hauer, M. Wieser, and N. Pfeifer. 2015. "Topo-Bathymetric LiDAR for Monitoring River Morphodynamics and Instream Habitats—A Case Study at the Pielach River." *Remote Sensing* 7, no. 5: 6160–6195. https://doi.org/10.3390/rs70506160.

Mansikkaniemi, H. 1970. *Deposits of Sorted Material in the Inarijoki-Tana River Valley in Lapland*. Vol. 49, 33. Publicationes Instituti Geographici Universitatis Turkuensis.

Marchamalo, M., M.-D. Bejarano, D. G. de Jalón, and R. M. Marín. 2007. "Fish Habitat Characterization and Quantification Using Lidar and Conventional Topographic Information in River Survey." In *Remote Sensing for Agriculture, Ecosystems, and Hydrology*, edited by C. M. U. Neale, M. Owe, and G. D'Urso, Proc. of SPIE 6742, 67420L. SPIE. https://doi.org/10.1117/12.737803.

McKean, J., D. Nagel, D. Tonina, et al. 2009. "Remote Sensing of Channels and Riparian Zones With a Narrow-Beam Aquatic-Terrestrial LIDAR." *Remote Sensing* 1, no. 4: 1065–1096. https://doi.org/10.3390/rs1041065.

Metsäniemi, T., P. Orell, A. Foldvik, J. Kuusela, M. Kurkilahti, and J. Erkinaro. 2025. "Mesohabitat Evaluation Reveals Variable Abundances and Habitat Choice in Juvenile Atlantic Salmon Across Diverse Habitats in the Main Stem of a Large Sub-Arctic River." *Ecology of Freshwater Fish* 34, no. 3: e70009. https://doi.org/10.1111/eff.70009.

Moradian, S., A. Torabi Haghighi, M. Asadi, and S. A. Mirbagheri. 2023. "Future Changes in Precipitation Over Northern Europe Based on a Multi-Model Ensemble From CMIP6: Focus on Tana River Basin." *Water Resources Management* 37, no. 6–7: 2447–2463. https://doi.org/10.1007/s11269-022-03272-4.

Morsy, S., A. a. Shaker, and A. El-Rabbany. 2018. "Using Multispectral Airborne LiDAR Data for Land/Water Discrimination: A Case Study at Lake Ontario, Canada." *Applied Sciences* 8, no. 3: 349. https://doi.org/10.3390/app8030349.

Mortensen, J. G., P. Y. Julien, B. Corsi, C. Radobenko, and T. Anderson. 2024. "Impacts of Hydrologic and Geomorphic Alteration to the Availability of Shallow, Low-Velocity Habitats in an Intensively Managed Arid-Land River." *River Research and Applications* 40, no. 10: 1808–1824. https://doi.org/10.1002/rra.4338.

Muraro, F., G. Dolcetti, A. Nichols, S. J. Tait, and K. V. Horoshenkov. 2021. "Free-Surface Behaviour of Shallow Turbulent Flows." *Journal of Hydraulic Research* 59, no. 1: 1–20. https://doi.org/10.1080/00221686.2020.1870007.

National Land Survey of Finland. 2015. *Orthophoto [Map]*. MapSite National Land Survey of Finland asiointi.maanmittauslaitos.fi./karttapaikka.

National Land Survey of Finland. 2024. *Topographic Database [Map]*. MapSite National Land Survey of Finland asiointi.maanmittauslaitos.fi./karttapaikka.

Nelson, J. M., J. P. Bennett, and S. M. Wiele. 2003. "Flow and Sediment-Transport Modeling." In *Tools in Fluvial Geomorphology*, 539–576. John Wiley & Sons, Ltd. https://doi.org/10.1002/0470868333.ch18.

Newson, M. d., D. M. Harper, C. L. Padmore, J. L. Kemp, and B. Vogel. 1998. "A Cost-Effective Approach for Linking Habitats, Flow Types and Species Requirements." *Aquatic Conservation: Marine and Freshwater Ecosystems* 8, no. 4: 431–446. https://doi.org/10.1002/(SICI)1099-0755(199807/08)8:4%3C431::AID-AQC302%3E3.0.CO;2-W.

NovAtel Inc. 2020. *Waypoint Software 8.90 User Manual* OM-20000166 Rev. 10. NovAtel Inc Accessed: 20 July 2026.

Ochs, K., R. P. Rivaes, T. Ferreira, and G. Egger. 2018. "Flow Management to Control Excessive Growth of Macrophytes – An Assessment Based on Habitat Suitability Modeling." *Frontiers in Plant Science* 9: 356. https://doi.org/10.3389/fpls.2018.00356.

O'Sullivan, A., B. Wegscheider, J. Helminena, et al. 2020. "Catchment-Scale, High-Resolution, Hydraulic Models and Habitat Maps – A Salmonid's Perspective." *Journal of Ecohydraulics* 6, no. 1: 53–68. https://doi.org/10.1080/24705357.2020.1768600.

Parasiewicz, P. 2007. "The MesoHABSIM Model Revisited." *River Research and Applications* 23, no. 8: 893–903. https://doi.org/10.1002/rra.1045.

Parasiewicz, P. 2008. "Application of MesoHABSIM and Target Fish Community Approaches to Restoration of the Quinebaug River, Connecticut and Massachusetts, USA." *River Research and Applications* 24, no. 4: 459–471. https://doi.org/10.1002/rra.1064.

Rawlins, M. A., H. Ye, D. Yang, A. Shiklomanov, and K. C. McDonald. 2009. "Divergence in Seasonal Hydrology Across Northern Eurasia: Emerging Trends and Water Cycle Linkages." *Journal of Geophysical Research* 114: D18119. https://doi.org/10.1029/2009JD011747.

Román, A., S. Heredia, A. E. Windle, A. Tovar-Sánchez, and G. Navarro. 2024. "Enhancing Georeferencing and Mosaicking Techniques Over Water Surfaces With High-Resolution Unmanned Aerial Vehicle (UAV) Imagery." *Remote Sensing* 16: 290. https://doi.org/10.3390/rs16020290.

Rosenfeld, J. 2003. "Assessing the Habitat Requirements of Stream Fishes: An Overview and Evaluation of Different Approaches." *Transactions of the American Fisheries Society* 132, no. 5: 953–968. https://doi.org/10.1577/t01-126.

Shannon, C. E., and W. Weaver. 1949. *The Mathematical Theory of Communication*. Vol. 132. University of Illinois Press – Urbana.

Sillero, N. 2011. "What Does Ecological Modelling Model? A Proposed Classification of Ecological Niche Models Based on Their Underlying Methods." *Ecological Modelling* 222, no. 8: 1343–1346. https://doi.org/10.1016/j.ecolmodel.2011.01.018.

Sinha, S. K., F. a. Sotiropoulos, and A. J. Odgaard. 1998. "Three-Dimensional Numerical Model for Flow Through Natural Rivers." *Journal of Hydraulic Engineering* 124, no. 1: 13–24. https://doi.org/10.1061/(ASCE)0733-9429(1998)124:1(13).

Takhtkeshha, N., G. Mandlburger, F. Remondino, and J. Hyyppä. 2024. "Multispectral Light Detection and Ranging Technology and Applications: A Review." *Sensors* 24, no. 5: 1669. https://doi.org/10.3390/s24051669.

Tamminga, A., and B. Eaton. 2018. "Linking Geomorphic Change due to Floods to Spatial Hydraulic Habitat Dynamics." *Ecohydrology* 11, no. 8: e2018. https://doi.org/10.1002/eco.2018.

Tonina, D., J. A. McKean, R. M. Benjankar, et al. 2019. "Mapping River Bathymetries: Evaluating Topobathymetric LiDAR Survey." *Earth

Surface Processes and Landforms 44, no. 2: 507–520. https://doi.org/10.1002/esp.4513.

Tonina, D., J. A. McKean, R. M. Benjankar, et al. 2020. "Evaluating the Performance of Topobathymetric LiDAR to Support Multi-Dimensional Flow Modelling in a Gravel-Bed Mountain Stream." *Earth Surface Processes and Landforms* 45, no. 12: 2850–2868. https://doi.org/10.1002/esp.4934.

van Rooijen, E., A. Siviglia, D. F. Vetsch, R. M. Boes, and D. Vanzo. 2024. "Quantifying Fluvial Habitat Changes due to Multiple Subsequent Floods in a Braided Alpine Reach." *Journal of Ecohydraulics* 9, no. 1: 1–21. https://doi.org/10.1080/24705357.2022.2105755.

Vezza P., L. Astegiano, and S. Fukuda. 2016. "Using Structure from Motion Techniques To Describe And Evaluate Instream Physical Habitat." Extended Abstract [Preprint], 11th ISE 2016, Melbourne, Australia.

Vezza, P., D. Ghia, and G. Fea. 2016. "Quantitative Habitat Models for the Conservation of the Endangered European Crayfish Austropotamobius Pallipes Complex (Astacoidea: Astacidae)." In *A Global Overview of the Conservation of Freshwater Decapod Crustaceans*, edited by T. Kawai and N. Cumberlidge, 339–358. Springer International Publishing. https://doi.org/10.1007/978-3-319-42527-6_12.

Vezza, P., P. Parasiewicz, M. Spairani, and C. Comoglio. 2014. "Habitat Modeling in High-Gradient Streams: The Mesoscale Approach and Application." *Ecological Applications* 24, no. 4: 844–861. https://doi.org/10.1890/11-2066.1.

Wallis, C., I. Maddock, F. Visser, and M. Acreman. 2012. "A Framework for Evaluating the Spatial Configuration and Temporal Dynamics of Hydraulic Patches." *River Research and Applications* 28, no. 5: 585–593. https://doi.org/10.1002/rra.1468.

Wegscheider, B., T. Linnansaari, and R. A. Curry. 2020. "Mesohabitat Modelling in Fish Ecology: A Global Synthesis." *Fish and Fisheries* 21, no. 5: 927–939. https://doi.org/10.1111/faf.12477.

Wegscheider, B., T. Linnansaari, M. Ndong, et al. 2024. "Fish Habitat Modelling in Large Rivers: Combining Expert Opinion and Hydrodynamic Modelling to Inform River Management." *Journal of Ecohydraulics* 9, no. 1: 68–86. https://doi.org/10.1080/24705357.2021.1938251.

Welber, M., J. le Coz, J. B. Laronne, et al. 2016. "Field Assessment of Noncontact Stream Gauging Using Portable Surface Velocity Radars (SVR)." *Water Resources Research* 52, no. 2: 1108–1126. https://doi.org/10.1002/2015WR017906.

Wheaton, J. M., K. A. Fryirs, G. Brierley, S. G. Bangen, N. Bouwes, and G. O'Brien. 2015. "Geomorphic Mapping and Taxonomy of Fluvial Landforms." *Geomorphology* 248: 273–295. https://doi.org/10.1016/j.geomorph.2015.07.010.

Woodget, A. S., R. Austrums, I. P. Maddock, and E. Habit. 2017. "Drones and Digital Photogrammetry: From Classifications to Continuums for Monitoring River Habitat and Hydromorphology." *WIREs Water* 4, no. 4: e1222. https://doi.org/10.1002/wat2.1222.

Wyrick, J., and G. Pasternack. 2012. *"Landforms of the Lower Yuba River," Prepared for the Yuba Accord River Management Team*. Vol. 92. University of California, Davis.

Wyrick, J. R., A. E. Senter, and G. B. Pasternack. 2014. "Revealing the Natural Complexity of Fluvial Morphology Through 2D Hydrodynamic Delineation of River Landforms." *Geomorphology* 210: 14–22. https://doi.org/10.1016/j.geomorph.2013.12.013.

Yan, W. Y., A. Shaker, and P. E. LaRocque. 2018. "Water Mapping Using Multispectral Airborne Lidar Data." *International Archives of the Photogrammetry, Remote Sensing and Spatial Information Sciences* XLII–3: 2047–2052. https://doi.org/10.5194/isprs-archives-XLII-3-2047-2018.

Yu, B., L. Chen, C. Yang, and P. Zhang. 2025. "Meso-Scale Habitat Distribution and Suitability Evaluation in Large River Systems: A Case Study of the Middle Yangtze River." *Ecohydrology* 18, no. 4: e70051. https://doi.org/10.1002/eco.70051.

Supporting Information

Additional supporting information can be found online in the Supporting Information section. **Table S1:** Change in mesohabitat as % of area from the Spring MQ scenario to Summer MQ scenario. The rows show the initial mesohabitats in Spring MQ, while the columns show the mesohabitats in Summer MQ. The cell values indicate the percentage of the spring mesohabitat area that has transitioned to the mesohabitat in question in the summer. **Table S2:** Change in mesohabitat as % of area from the Summer MQ scenario to Autumn MQ scenario. The rows show the initial mesohabitats in Summer MQ, while the columns show the mesohabitats in Autumn MQ. The cell values indicate the percentage of the summer mesohabitat area that has transitioned to the mesohabitat in question in the autumn.